Mathematical descriptions of nematic polymers in the monolayer limit

by
Joohee Lee

A dissertation submitted to the faculty of the University of North Carolina at Chapel Hill in partial fulfillment of the requirements for the degree of Doctor of Philosophy in the Department of Mathematics.

Chapel Hill
2007

Approved by,
Advisor: M. Gregory Forest
Reader: Tim Elston
Reader: Jingfang Huang
Reader: William M. Mullins
Reader: Ruhai Zhou

ABSTRACT

JOOHEE LEE: MATHEMATICAL DESCRIPTIONS OF NEMATIC POLYMERS IN THE MONOLAYER LIMIT**.**

(Under the direction of M. Gregory Forest.)

Monolayer films of liquid crystalline polymers (LCPs) are modeled with a two dimensional (2D) analog of the Doi-Hess (1981, 1976) kinetic model. In this dissertation, we focus on the analysis of the Doi-Hess Smoluchowski equation for the orientational distribution of LCPs, and an understanding of the distinctions which arise due to 2D confinement relative to results for full orientational space distributions. In Chapter 2, we study the mesoscopic model which approximates the Doi-Hess kinetic model, based on a second-moment closure. In this setting, we establish a more complete solution to the classical problem of how orientational degeneracy of quiescent nematic equilibria breaks in weak shear, and we determine the distinctions between two versus three dimensional sheared nematic-liquids. We give the first proof that limit cycles, known as tumbling orbits, must arise beyond the parameter boundary for the steady-unsteady transition. Finally, we show the shear-perturbed 2D phase diagram is significantly more robust to closure approximations than the 3D system. In Chapter 3, we solve a two dimensional Smoluchowski equation which is the extended Doi-Hess model for magnetic nano-rod dispersions in linear flows. We obtain closed-form representations of all steady state solutions in terms of Boltzmann distributions of the Smoluchowski equation. This method yields an exact, finite-dimensional reduction of the infinite-dimensional PDE, from which we construct bifurcation diagrams for all equilibria without external fields.

ACKNOWLEDGMENTS

I would like to thank my advisor Professor Gregory Forest, who guided me to see both trees and the forest during my graduate education. I am also grateful to Professors Ruhai Zhou, Qi Wang, Bill Mullins, and Zhenlu Cui for helping me to deepen my understanding of modeling of nematic polymers. My special appreciation goes to my family for their love and support. I also acknowledge research support provided by the Army Research Office and the National Science Foundation.

TABLE OF CONTENTS

LIST OF FIGURES

Chapter 1

Introduction

Liquid crystalline polymers (rigid macromolecules dispersed in a solvent) form ordered phases, which are intermediate between liquids and crystalline solids, on the scale of microns due to excluded volume interactions of approximately 10^5 macromolecules. Liquids have only short-range order and crystalline solids ideally have perfect order both with respect to the position and orientation of their component molecules. These ordered "mesophases" are systems in which a liquid-like order exists at least in one direction of space and in which some degree of anisotropy is present. There are three types of liquid-crystalline structures: nematic, cholesteric, and smectic (de Gennes and Prost, 1993). The nematic liquid crystalline phase has the simplest ordering. It possesses long range orientational order in one direction like a solid but only a short range positional order like a liquid. A cholesteric is similar to a nematic but the direction in space is twisted helically. A smectic phase has structures with layered ordering.

In the early 1970's, there was the first commercialization of Kevlar aromatic polyamide fiber. This fiber can be almost as stiff and as strong as steel with 20% of the density. In addition, it has high thermal stability and strong chemical resistance. Kevlar is used to produce bullet proof vests, ropes, cables and high performance sporting goods like tennis racquets, where high strength and light weight are essential. Optical properties of liquid crystals are extremely sensitive to external perturbations. The color of cholesteric liquid crystals varies with temperature. These properties have been exploited to build sensitive

temperature devices for medical applications. Twisted-nematic displays have been commercialized successfully in the digital watch, hand-held calculator and computer display industry.

Since the rheological properties of nematic liquid crystals are strongly affected by the dynamic behavior of the molecular alignment, it is very important to know how to control the orientation. The Doi-Hess model for rod-like molecules has been very successful in describing the hydrodynamics of liquid crystalline polymers. This model provides an evolution equation for the orientational probability distribution function of a single molecule. The rotational motion of a rod is severely constrained by surrounding rods. Interactions between molecules are modeled by a mean-field excluded-volume potential. The model also includes flow-coupling and Brownian diffusion for the orientational distribution. The system forms a nematic phase, distinguished by a partially ordered, anisotropic orientational distribution, above a certain concentration of rods. Otherwise the system is in an isotropic phase in which the orientation of the rod is completely random. An intermediate range of concentrations admits bi-stability.

The focus of this dissertation is on the analysis of the two-dimensional Doi-Hess model, which is physically motivated by monolayer films (Maruyama *et al.*, 1998), and an understanding of the distinctions which arise due to 2D confinement relative to results for full orientational space distributions. The Doi-Hess kinetic model gives rise to a Smoluchowski equation for the orientational probability distribution function. A mesoscopic approximation based on moment closure rules has been introduced to reduce the complexity of the kinetic model (which is an infinite-dimensional dynamical system) to a low-dimensional, more tractable, dynamical system. In Chapter 2, we begin with the mesoscopic model to study what survives from orientational degeneracy of the quiescent nematic phase as an external perturbation is turned on. We solve the two-dimensional weak shear problem analytically and obtain shear-perturbed 2D phase diagrams numerically for various second-moment closures.

The molecules of liquid crystals are anisotropic not only in shape but also with respect

to charge. This makes their orientation affected by electric and magnetic fields, and also makes them optically birefringent. Those properties are used in developing display devices. The Doi-Hess model for rigid rod-like nematic polymers was extended to magnetic nano-rod dispersions by Bhandar and Wiest (Bhandar and Wiest, 2003). The model includes magnetic field effects in addition to Browninan diffusion, flow-coupling and excluded-volume interactions. In Chapter 3, we study the extended Smoluchowski equation for magnetic dispersions. We obtain the steady state solution of the Smoluchowski equation for general linear flows in semi-implicit form. This is an exact reduction of the PDE to a two-dimensional system, a result first achieved formally by Onsager (Onsager, 1949) and later made rigorous by Constantin and collaborations (Constantin *et al.*, 2004). We also construct bifurcation diagrams for the case of no external fields.

Chapter 2

Alignment and rheo-oscillator criteria for sheared nematic polymer films in the monolayer limit

2.1 Introduction

Hess (Hess, 1976) and Doi (Doi, 1981) proposed the nematic liquid crystalline model which provides an evolution equation for the orientational probability density function of rod-like molecules in a laminar flow field. Marrucci and Maffetonne developed an insightful analysis of the two-dimensional form of this model to understand the steady-unsteady transition in weak shear (Marrucci and Maffetone, 1989). For the case of two-dimensional nematic polymers, Maffetonne and Crescitelli (Maffetone and Crescitelli, 1994, 1995) analyzed a simplified constitutive equation in order to examine closure approximations and numerically explored bifurcations of the kinetic model equation using the continuation software AUTO (Doedel *et al.*, 1998; Ermentrout, 2002). These model predictions were applied to experiments on monolayers of nematic polymers performed in Fuller's group (Maruyama *et al.*, 1998; Yim *et al.*, 2001). Faraoni and Grosso *et al.* (Faraoni *et al.*, 1999), following initial results of Larson and Öttinger (Larson and Öttinger, 1991), revealed various bifurcations of the 3-dimensional Doi model using spherical harmonic

expansions and AUTO. Forest, Wang and Zhou (Forest *et al.*, 2003, 2004) provided the 3-dimensional Doi-Hess kinetic phase diagram, giving all attracting steady, periodic, and irregular orientational distributions versus shear rate and polymer concentration.

Amid all of these results, one of the classical issues of anisotropic molecular liquids, dating back to Onsager and de Gennes, is *what survives from orientational degeneracy of the quiescent nematic phase just as an external field perturbation is turned on.* This issue was bypassed in the continuum liquid crystal theory of Leslie and Ericksen, which did not involve an excluded-volume potential. The Leslie material parameters produced either a shear flow-aligning or a tumbling liquid crystalline fluid, with no freedom to transition between them, by varying experimental conditions such as volume fraction of the nematic polymer solvent mixture or the shear rate. Furthermore, there was no dynamics without an external field (hydrodynamic, electric or magnetic). For liquid crystalline polymers, however, the experimental evidence was mounting in the 1980's for not only an equilibrium 1^{st}-order isotropic-nematic phase transition, but a shear rate-dependent, steady-unsteady transition (Kiss & Porter '78, '80) which was accompanied by sign change in the first normal stress difference. The kinetic theory of Hess and Doi, and mesoscopic second-moment tensor approximations of Landau-de Gennes type (de Gennes & Prost '93, Beris & Edwards '95), became the focus of intense theoretical and numerical study to explain the shear behavior of nematic polymers. We refer the reader to several informative papers (Hinch & Leal '76, Marrucci & Greco '93, Larson & Öttinger '91, Burghardt '98, Berry & Tan '01, Rey & Denn '02, Forest & Wang '03, Kroger '04).

This chapter addresses the question posed above for a model 2 dimensional liquid, physically motivated by monolayer films. Thin films of liquid crystalline polymers have been of considerable interest due to their stability and nonlinear optical properties compared to that of low molecular weight materials (Maffetone *et al.*, 1996). Maffetone *et al.* (Maffetone *et al.*, 1996) showed the two-dimensional model proposed by Marrucci and Maffetone (Marrucci and Maffetone, 1989) could quantitatively predict the dynamic

behavior of thin films under planar extensional flow. Maruyama *et al.* (Maruyama *et al.*, 1998) examined the orientation dynamics of monolayer nematic polymer films for both extensional and simple shear flows. They obtained evidence of wagging (finite amplitude oscillations) and flow alignment in simple shear flow, depending on shear rate.

There is a *qualitative* difference between two-dimensional and three-dimensional isotropic-nematic transitions. In three dimensions, the transition is first order, discontinuous and the phase diagram exhibits hysteresis. On the other hand, mean field theory predicts that the transition should be second-order and continuous in two dimensions (cf. (Faraoni *et al.*, 1999; Forest *et al.*, 2004; Marrucci and Maffetone, 1989), Fig. 2.1, 2.2). The other important feature distinctions are "degree of degeneracy" of nematic phases, and the discrete number of ordered phases: In three dimensions, there are two types of ordered phases with distinct degrees of orientation and different "shapes" of the orientational distribution with one stable and the other unstable. The unstable branch does play a role in shear-dependent bifurcation diagrams as those branches subsequently collide with others (Forest and Wang, 2003). In two dimensions, there is only one nematic phase; the "lower branch" is identical to the upper branch associated with a $\mathbb{Z}_2$-symmetry (Golubitsky and Schaeffer, 1985) unique to two-dimensional liquids, explained below. Thus, subsequent bifurcations in shear flows with other applied fields will be qualitatively distinct.

The purpose of this chapter is to analytically solve the two-dimensional weak shear problem. That is, we aim to rigorously explain how the 2D quiescent phase diagram versus dimensionless concentration N extends in the two parameter space of (N, Pe), where Pe is the dimensionless shear rate, and to understand whether the extreme sensitivity to closure rule of 3-dimensional nematic liquids (Forest and Wang, 2003) also obtains in two-dimensional orientational dynamics.

2.2 Kinetic theory and mesoscopic models

Let $f(\mathbf{m}, t)$ be the orientational probability distribution function (PDF) that the axis of revolution of the molecule has an orientation given by the unit vector $\mathbf{m}$=$(\cos\theta, \sin\theta)$ at time t. The Doi-Hess theory gives an evolution equation for the PDF $f(\mathbf{m}, t)$,

$$\frac{\partial f}{\partial t} = D_r^0 \frac{\partial}{\partial \mathbf{m}} \cdot [\frac{\partial f}{\partial \mathbf{m}} + \frac{f}{k_B T} \frac{\partial V_{MS}}{\partial \mathbf{m}}] - \frac{\partial}{\partial \mathbf{m}} \cdot (\dot{\mathbf{m}} f), \tag{2.1}$$

where D_r^0 is an averaged rotary diffusivity or relaxation rate, k_B is the Boltzman constant, T is the absolute temperature. The first term in (2.1) is Brownian diffusion on the sphere. The second term is due to molecule interactions, explained further below. The third term is the flow coupling through the velocity gradient,

$$\nabla \mathbf{v} = \mathbf{\Omega} + \mathbf{D}, \tag{2.2}$$

where $\mathbf{\Omega}$ is the vorticity tensor and $\mathbf{D}$ is the rate of strain tensor given by

$$\mathbf{\Omega} = \frac{1}{2}(\nabla \mathbf{v} - \nabla \mathbf{v}^T), \ \mathbf{D} = \frac{1}{2}(\nabla \mathbf{v} + \nabla \mathbf{v}^T), \tag{2.3}$$

$$\dot{\mathbf{m}} = \mathbf{\Omega} \cdot \mathbf{m} + a[\mathbf{D} \cdot \mathbf{m} - \mathbf{D} : \mathbf{mmm}]. \tag{2.4}$$

This is the so-called Jeffery orbit for spheroids in Stokes flow in a viscous solvent, where $-1 \leq a \leq 1$ is the molecular shape parameter related to the molecular aspect ratio r by

$$a = \frac{r^2 - 1}{r^2 + 1}. \tag{2.5}$$

We assume two-dimensional simple shear flow $\mathbf{v} = \dot{\gamma}(y, 0)$, where $\dot{\gamma}$ is the shear rate, for which the rate of strain and vorticity tensors are

$$\begin{aligned} \mathbf{D} &= \dot{\gamma}\tilde{\mathbf{D}}, & \mathbf{\Omega} &= \dot{\gamma}\tilde{\mathbf{\Omega}} \\ \tilde{\mathbf{D}} &= \tfrac{1}{2}\begin{pmatrix} 0 & 1 \\ 1 & 0 \end{pmatrix}, & \tilde{\mathbf{\Omega}} &= \tfrac{1}{2}\begin{pmatrix} 0 & 1 \\ -1 & 0 \end{pmatrix}. \end{aligned} \tag{2.6}$$

In (2.1), V_{MS} is the Maier-Saupe excluded-volume potential with strength proportional to the dimensionless polymer concentration N,

$$V_{MS} = -2Nk_BT\mathbf{mm} :< \mathbf{mm} > . \tag{2.7}$$

The second moment $\mathbf{M}$ of the PDF $f(\mathbf{m}, t)$ is prominent in any connections of theory to experimental data:

$$\mathbf{M} =< \mathbf{mm} >= \int_0^{\pi} \mathbf{mm} f(\mathbf{m}, t) d\mathbf{m}. \tag{2.8}$$

The map between light scattering intensity I in the plane of $\mathbf{m}$ and the orientational distribution function f is (Maruyama *et al.*, 1998)

$$I = \frac{2\pi hs}{\omega}, \tag{2.9}$$

where h is the monolayer thickness, ω is the wavelength of the incident light and s is the Hermans orientation parameter determined from $\mathbf{M}$, equation (2.15). The mesoscopic orientation tensor $\mathbf{Q} = \mathbf{M} - \frac{1}{2}\mathbf{I}$ is the traceless part of $\mathbf{M}$. Similarly, one represents higher moments of f with this bracket notation.

The nematodynamical equation for $\mathbf{Q}$ is derived from (2.1):

$$\begin{aligned} \frac{d}{dt}\mathbf{Q} &= \mathbf{\Omega}\cdot\mathbf{Q} - \mathbf{Q}\cdot\mathbf{\Omega} + a[\mathbf{D}\cdot\mathbf{Q} + \mathbf{Q}\cdot\mathbf{D}] + a\mathbf{D} - 2a\mathbf{D} :< \mathbf{mmmm} > \\ &\quad -6\mathbf{D}_r^0[\mathbf{Q} - N(\mathbf{Q} + \tfrac{1}{2}\mathbf{I})\cdot\mathbf{Q} + N\mathbf{Q} :< \mathbf{mmmm} >]. \end{aligned} \tag{2.10}$$

The variable coefficients in the linear Smoluchowski equation (2.1) translate to nonlinearity and coupling between moments in the moment equations, so that any finite moment truncation requires some closure approximation. Following tradition in polymeric systems, and motivated by a closed theory for the physically measurable second moment properties, many models have posited a closed equation for $\mathbf{M}$, respectively $\mathbf{Q}$. The Doi closure rule assumes $(\bullet) :< \mathbf{mmmm} >= (\bullet) :< \mathbf{mm} >< \mathbf{mm} >$; other closures due to Tsuji-Rey and Hinch-Leal are discussed and analyzed below.

We now non-dimensionalize the flow field and orientation dynamics (2.10) using the nematic relaxation time scale $(D_r^0)^{-1}$. The key dimensionless parameters are then the Peclet number $Pe = \frac{\dot{\gamma}}{D_r^0}$, the shear rate normalized relative to nematic relaxation rate, and the dimensionless concentration N. Hereafter, we work in dimensionless time $\tilde{t} = tD_r^0$.

2.3 Q-tensor representations

2.3.1 Component representation

A component representation is a standard matrix representation with respect to a chosen coordinate system. The typical Cartesian representation of $\mathbf{Q}$ satisfies a symmetry constraint $Q_{xy} = Q_{yx}$ and a trace zero constraint $Q_{xx} + Q_{yy} = 0$ having two independent degrees of freedom. The symmetric traceless matrices form a two-dimensional vector space with standard basis

$$\mathbf{Q}^{(1)} = \begin{pmatrix} 1 & 0 \\ 0 & -1 \end{pmatrix}, \quad \mathbf{Q}^{(2)} = \begin{pmatrix} 0 & 1 \\ 1 & 0 \end{pmatrix}, \tag{2.11}$$

which have eigenvector frames $\{(1,0),(0,1)\}$ and $\{(1,1),(1,-1)\}$, respectively corresponding to eigenvalues 1 and -1. In this basis, the two independent components Q_{xx}, Q_{xy} are evident:

$$\mathbf{Q} = Q_{xx}\mathbf{Q}^{(1)} + Q_{xy}\mathbf{Q}^{(2)}. \tag{2.12}$$

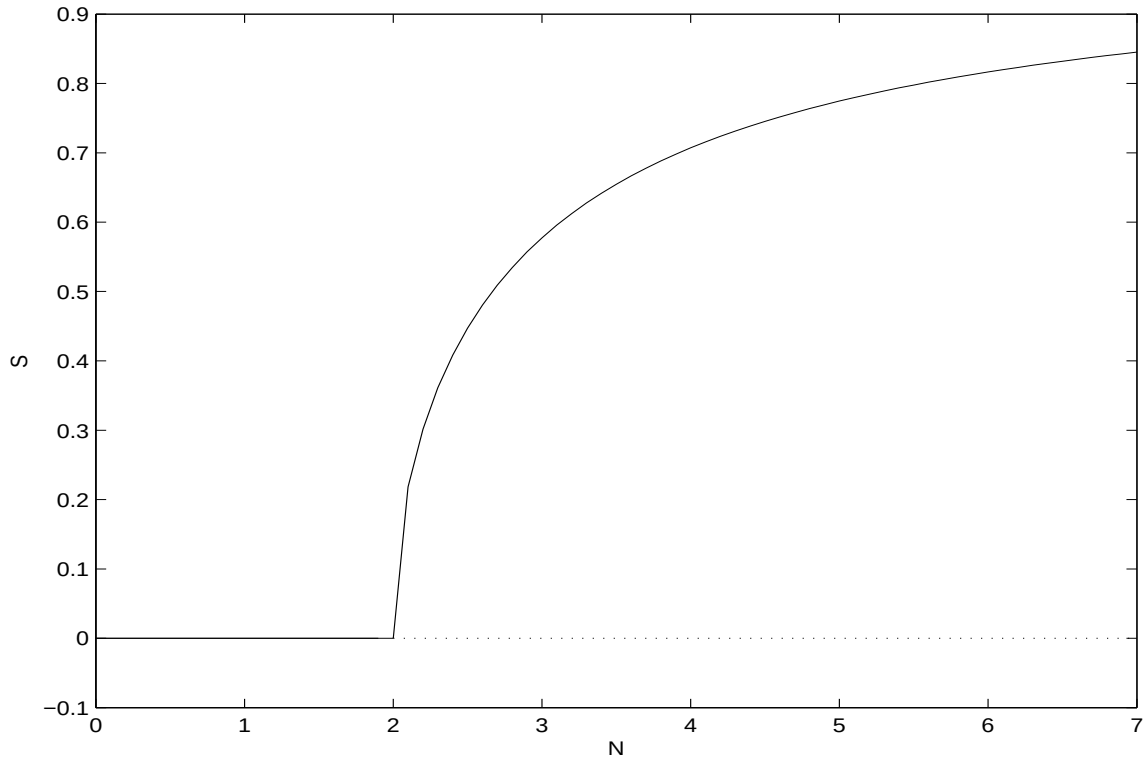

Figure 2.1: Isotropic-nematic transition diagram without flow of the 2D Doi closure model. The order parameter S is plotted against dimensionless concentration N. The stable isotropic solution becomes unstable and the stable nematic branch is born at $N = 2$. Solid (dashed) curves denote stable (unstable) equilibria.

For the Doi closure, the nematodynamic model (2.10) takes the following form using the component representation (2.12):

$$\begin{aligned} \dot{Q_{xx}} &= -6Q_{xx}(1 - \tfrac{N}{2} + 2N(Q_{xx}^2 + Q_{xy}^2)) + Pe(Q_{xy} - 2aQ_{xx}Q_{xy}) \\ \dot{Q_{xy}} &= -6Q_{xy}(1 - \tfrac{N}{2} + 2N(Q_{xx}^2 + Q_{xy}^2)) + Pe(-Q_{xx} + \tfrac{a}{2} - 2aQ_{xy}^2). \end{aligned} \tag{2.13}$$

2.3.2 Spectral representation

Since $\mathbf{Q}$ is symmetric, the eigenvectors of $\mathbf{Q}$ form an orthonormal basis of $\mathbb{R}^2$. From the spectral theorem, if d_i is the eigenvalue associated with eigenvector $\mathbf{n}_i$, then

$$\mathbf{Q} = \sum (d_i - \frac{1}{2})\mathbf{n}_i\mathbf{n}_i, \quad d_1 + d_2 = 1, \sum \mathbf{n}_i\mathbf{n}_i = \mathbf{I}. \tag{2.14}$$

It follows that $\mathbf{Q}$ has the spectral representation

$$\mathbf{Q} = s(\mathbf{n}_1\mathbf{n}_1 - \frac{\mathbf{I}}{2}),\ s = d_1 - d_2 = 2d_1 - 1, \tag{2.15}$$

where $\frac{1}{2}s$ is an eigenvalue of $\mathbf{Q}$ associated with major director $\mathbf{n} = (\cos\theta, \sin\theta)$.

The map between (Q_{xx}, Q_{xy}) and (s, θ) is

$$\begin{aligned} Q_{xx} &= \tfrac{s}{2}\cos 2\theta \\ Q_{xy} &= \tfrac{s}{2}\sin 2\theta, \end{aligned} \tag{2.16}$$

and the Doi closure model (2.13) has an equivalent form:

$$\begin{aligned} \dot{\theta} &= -\tfrac{Pe}{2}(1 - \tfrac{a}{s}\cos 2\theta) \\ \dot{s} &= -3(N(s^2-1)+2)s + aPe(1-s^2)\sin 2\theta. \end{aligned} \tag{2.17}$$

From (2.17), the quiescent 2D nematic liquid ($Pe \equiv 0$) has equilibria $s = 0$ (the isotropic state $\mathbf{Q} = \mathbf{0}$) for all N, and nematic equilibria

$$s_\pm = \pm\sqrt{1 - \frac{2}{N}}, \tag{2.18}$$

for $N > 2$. From the first equation of (2.17), the director for nematic equilibria is arbitrary, which is known as orientational degeneracy. From the second equation of (2.17), one easily finds $s = 0$ is stable for $N < 2$ and unstable for $N \geq 2$, whereas $s_\pm$ are stable in the order parameter direction, while neutral in the θ direction. This explains Fig. 2.1.

In any closure model, (2.17) takes the form $\dot{\theta} = -\frac{Pe}{2}(1 - \lambda_L \cos 2\theta)$, where λ_L is the 2-dimensional analog of the Leslie alignment parameter. This parameter gives an explicit criterion for steady equilibria ($|\lambda_L| > 1$) versus unsteady behavior ($|\lambda_L| < 1$), and also encodes the closure rule. For the Doi closure, $\lambda_L = \frac{a}{s}$; for other closures, the form is given in Appendix A.2.

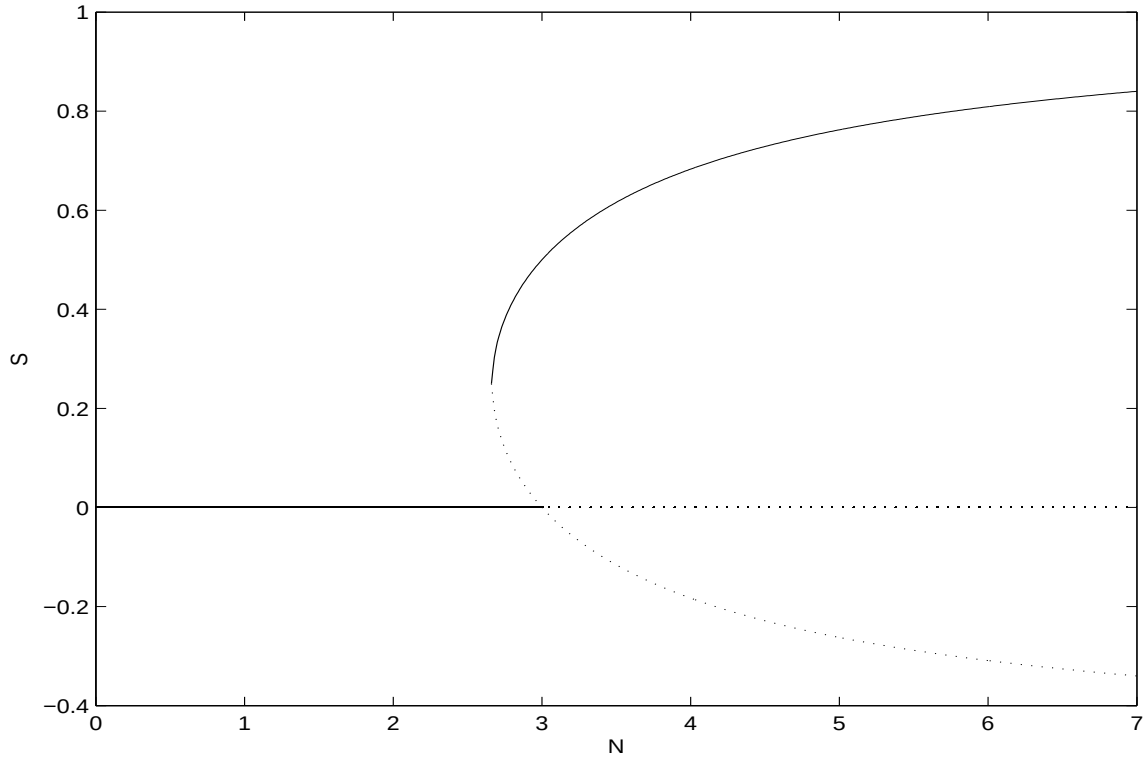

Figure 2.2: Isotropic-nematic transition diagram for 3D nematic liquids. The equilibrium branches $s_0 = 0$ and $s_\pm = \frac{1\pm3\sqrt{1-\frac{8}{3N}}}{4}$ are given for the Doi closure model with solid (dotted) curves representing stable (unstable) equilibria.

We now make note of a discrete symmetry that is special to two dimensions, which has consequences for the isotropic-nematic phase diagram as shown in Fig. 2.1. From (2.14), $\mathbf{Q}$ can be represented by either $s_+, \mathbf{n}_1$ or $s_-, \mathbf{n}_2$, and the representations are identical:

$$\mathbf{Q} \;=\; s_+\Big(\mathbf{n}_1\mathbf{n}_1 - \frac{1}{2}\mathbf{I}\Big) = -s_+\Big(\mathbf{n}_2\mathbf{n}_2 - \frac{1}{2}\mathbf{I}\Big) = s_-\Big(\mathbf{n}_2\mathbf{n}_2 - \frac{1}{2}\mathbf{I}\Big). \tag{2.19}$$

This implies, in stark contrast to the 3-dimensional nematic equilibrium sets, that there is only one nematic branch, i.e. the s_--branch is identical to the s_+-branch, thus the terminology $\mathbb{Z}_2$-symmetry (Golubitsky and Schaeffer, 1985). This observation has significant physical consequences, captured in the bifurcation structure associated with simultaneous instability of the isotropic branch and onset of the nematic branch. This bifurcation is depicted in Fig. 2.1 and is called a pitchfork bifurcation with $\mathbb{Z}_2$-symmetry. By com-

parison with Fig. 2.2 for 3-dimensional molecular liquids, the dotted lower branch of unstable "oblate" nematic phases does not exist in 2D. Thus, the only orientation state for which the major director is not unique (the definition of a defect) is the isotropic state, $\mathbf{Q} = \mathbf{0}$. In 3D, there are additional phases where the major director lies on a circle, giving another class of defects.

2.4 Weak-shear solvability conditions for persistence of equilibria

We now follow (Forest *et al.*, 2003) to assess persistence of the isotropic and S^1-invariant branches of solutions in Fig. 2.1 in the presence of a weak shear flow. This is accomplished by parametrizing all equilibria of (2.18) and then deriving solvability conditions at next order in the weak flow parameter Pe.

Assume weak shear, $Pe \ll 1$, and expand $\mathbf{Q}$ in powers of Pe:

$$\mathbf{Q} = \mathbf{Q}_0 + Pe\mathbf{Q}_1 + Pe^2\mathbf{Q}_2 + \cdots . \tag{2.20}$$

We seek those equilibria $\mathbf{Q}_0$ which survive in weak shear and $\mathbf{Q}_1$ is the leading shear-dependent correction. At order Pe, for any mesoscopic tensor model (2.10), $\mathbf{Q}_1$ must satisfy a linearized tensor-operator equation,

$$\mathbf{A}_1(\mathbf{Q}_0) \cdot \mathbf{Q}_1 = \mathbf{r}_1(\mathbf{Q}_0), \tag{2.21}$$

where $\mathbf{A}_1(\mathbf{Q}_0)$ corresponds to rotational diffusion and linearized Maier-Saupe potential, and $\mathbf{r}_1(\mathbf{Q}_0)$ is the linearized flow perturbation. With the Doi closure model, these oper-

ators are given by

$$\begin{aligned}
\mathbf{A}_1(\mathbf{Q}_0)\cdot\mathbf{Q}_1 &= 6[\mathbf{Q}_1 - N(\mathbf{M}_0\cdot\mathbf{Q}_1 + \mathbf{Q}_1\cdot\mathbf{Q}_0) \\
&\quad +N((\mathbf{Q}_0:\mathbf{M}_0)\mathbf{Q}_1 + (\mathbf{Q}_0:\mathbf{Q}_1)\mathbf{M}_0 + (\mathbf{Q}_1:\mathbf{M}_0)\mathbf{M}_0)], \\
\mathbf{r}_1(\mathbf{Q}_0) &= \tilde{\mathbf{\Omega}}\cdot\mathbf{Q}_0 - \mathbf{Q}_0\cdot\tilde{\mathbf{\Omega}} + a[\tilde{\mathbf{D}}\cdot\mathbf{Q}_0 + \mathbf{Q}_0\cdot\tilde{\mathbf{D}}] \\
&\quad +a\tilde{\mathbf{D}} - 2a\tilde{\mathbf{D}}:\mathbf{M}_0\mathbf{M}_0
\end{aligned} \tag{2.22}$$

where $\mathbf{M}_0 = \mathbf{Q}_0 + \frac{1}{2}\mathbf{I}$. The Fredholm alternative theorem yields the weak-shear solvability condition (Forest *et al.*, 2003; Kuzuu and Doi, 1983):

$$\mathbf{r}_1(\mathbf{Q}_0) \perp \mathcal{N}[\mathbf{A}_1^T(\mathbf{Q}_0)], \tag{2.23}$$

where $\mathcal{N}$ denotes the null space of the matrix $\mathbf{A}_1^T$. This solvability condition must be satisfied by these quiescent states $\mathbf{Q}_0$ in (2.18) which persist as steady states in weak shear, arising either from the stable nematic equilibrium or isotropic equilibria.

2.4.1 The shear-perturbed, nearly isotropic branch

The isotropic steady state perturbs at $O(Pe)$ to a unique, explicit branch of equilibria,

$$\mathbf{Q} = \mathbf{0} + Pe\frac{a}{3(2-N)}\tilde{\mathbf{D}} + O(Pe^2), \tag{2.24}$$

where $\tilde{\mathbf{D}}$ is the normalized rate-of-strain for pure shear. The directors of $\mathbf{Q}$ are

$$\mathbf{n}_1 = (1,1), \quad \mathbf{n}_2 = (1,-1), \tag{2.25}$$

with corresponding distinct order parameters

$$d_1 = \frac{1}{2} + \frac{a}{6(2-N)}Pe, \quad d_2 = \frac{1}{2} - \frac{a}{6(2-N)}Pe. \tag{2.26}$$

Note that the Leslie alignment angle $\theta \equiv \frac{\pi}{4}$ from $\mathbf{n}_1 = (1,1) = (\cos\theta, \sin\theta)$, at leading order in Pe for all concentrations away from $N = 2$. This is consistent with 3D kinetic (Forest *et al.*, 2004) and mesoscopic (Forest *et al.*, 2003) analysis. The degree of anisotropy is measured by $|d_1 - d_2|$, and for $|N - 2| > Pe$, the Flory order parameter $|d_1 - d_2|$ is proportional to the presumed weak normalized shear rate, Pe.

The next order solvability condition,

$$\mathbf{A}_2(\mathbf{Q}_0, \mathbf{Q}_1) \cdot \mathbf{Q}_2 = \mathbf{r}_2(\mathbf{Q}_0, \mathbf{Q}_1), \tag{2.27}$$

determines stability of the persistent equilibria (2.24). For the Doi closure model, the operators in (2.27) are given by

$$\begin{aligned}
\mathbf{A}_2(\mathbf{Q}_0, \mathbf{Q}_1) \cdot \mathbf{Q}_2 &= 6[\mathbf{Q}_2 - N(\mathbf{M}_0 \cdot \mathbf{Q}_2 + \mathbf{Q}_2 \cdot \mathbf{Q}_0) \\
&\quad + N(\mathbf{Q}_0 : \mathbf{M}_0\mathbf{Q}_2 + (\mathbf{Q}_2 : \mathbf{M}_0 + \mathbf{Q}_0 : \mathbf{Q}_2)\mathbf{M}_0)], \\
\mathbf{r}_2(\mathbf{Q}_0, \mathbf{Q}_1) &= \tilde{\mathbf{\Omega}} \cdot \mathbf{Q}_1 - \mathbf{Q}_1 \cdot \tilde{\mathbf{\Omega}} + a[\tilde{\mathbf{D}} \cdot \mathbf{Q}_1 + \mathbf{Q}_1 \cdot \tilde{\mathbf{D}}] \\
&\quad - 2a(\tilde{\mathbf{D}} : \mathbf{M}_0\mathbf{Q}_1 + \tilde{\mathbf{D}} : \mathbf{Q}_1\mathbf{M}_0) \\
&\quad + 6[N\mathbf{Q}_1 \cdot \mathbf{Q}_1 - N((\mathbf{Q}_1 : \mathbf{M}_0 + \mathbf{Q}_0 : \mathbf{Q}_1)\mathbf{Q}_1 + \mathbf{Q}_1 : \mathbf{Q}_1\mathbf{M}_0)].
\end{aligned} \tag{2.28}$$

The operator $-\mathbf{A}_2$ has explicit linearized eigenvalues,

$$\lambda_1 \approx \lambda_2 = -3(2 - N) + O(Pe), \tag{2.29}$$

from which we deduce the shear-perturbed isotropic branch is stable for $N < 2$ and unstable for $N > 2$. These results give detailed information about the corresponding solution branches with $|Q_{xx}| \ll 1$ in Fig. 2.4 (Leslie angles) and Fig. 2.5, where solid (dotted) lines indicate stable (unstable) states. The transition region surrounding $N = 2$ is treated next.

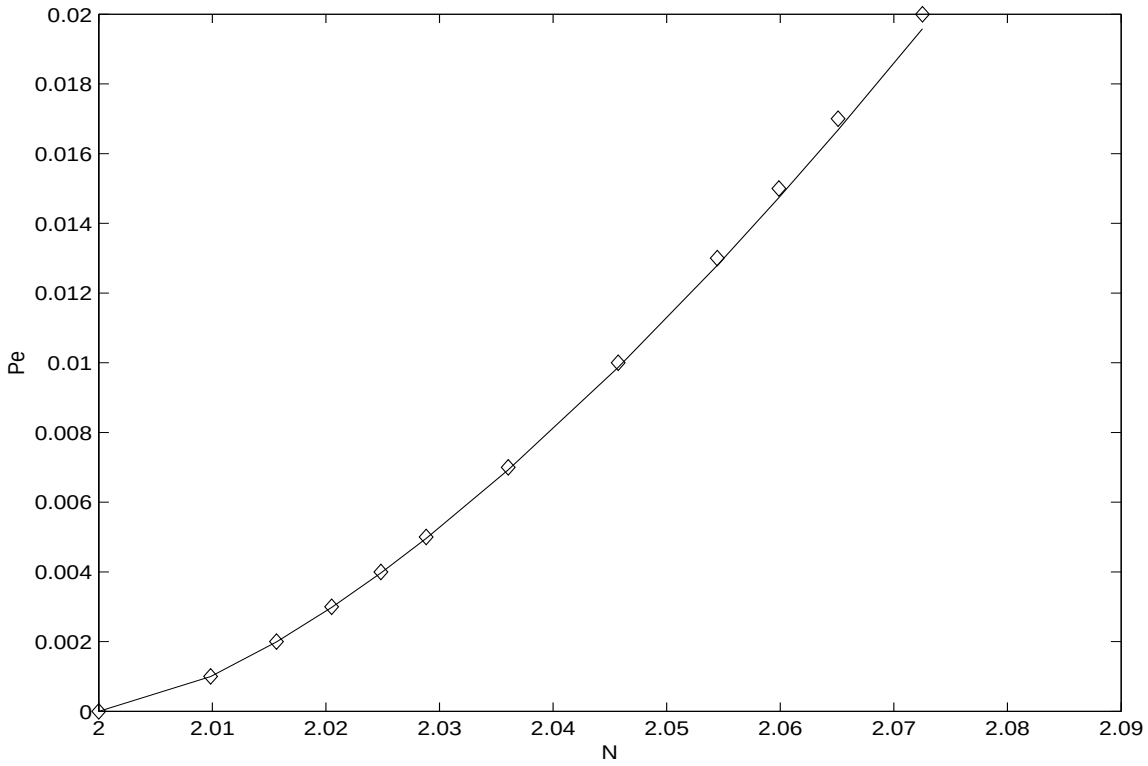

Figure 2.3: The scaling behavior of the bifurcation point LP2, Fig. 2.5. The solid line is the analytical prediction, while the diamonds represent LP2 points obtained by AUTO. These bifurcation points represent the locus of turning points where the unstable isotropic branch and the unstable nematic branch are connected.

2.4.2 Persistence of the I-N transition, i.e. the $\mathbb{Z}_2$-symmetric pitchfork bifurcation

Near $N = 2$, the expansion (2.24) breaks down. This suggests we need a different scaling in (2.20), e.g. a Pe^{α} expansion in a neighborhood of the isotropic-nematic transition $N = 2$ for small Pe. See, Doi and Larson (See *et al.*, 1990) calculated this scaling, $Pe^{\frac{1}{2}}$, in the 3-dimensional case, which was confirmed by Forest, Wang and Zhou (Forest *et al.*, 2004) in their analysis of all solution branches.

To capture the scaling behavior for persistence of the $\mathbb{Z}_2$-symmetric pitchfork bifurcation at $N = 2$, in Fig. 2.1, we impose two solvability conditions from (2.13). First, persistence of equilibria will yield 2 scalar equations, then a neutral (or marginal) stability condition on these equilibria yields a third condition. Together, these criteria give

3 conditions in (Q_{xx}, Q_{xy}, N, Pe), whose 1-parameter family of solutions gives the curve of persistent bifurcation values (N, Pe), together with the **Q**-tensor along the curve. For the Doi closure, the equilibria at leading order in Pe satisfy

$$H_1 = -6Q_{xx}(1 - \frac{N}{2} + 2N(Q_{xx}^2 + Q_{xy}^2)) = 0 \tag{2.30}$$

$$H_2 = -6Q_{xy}(1 - \frac{N}{2} + 2N(Q_{xx}^2 + Q_{xy}^2)) + Pe\frac{a}{2} = 0. \tag{2.31}$$

The marginal stability condition (See *et al.*, 1990) is

$$DET\frac{\partial(H_1, H_2)}{\partial(Q_{xx}, Q_{xy})} = 0. \tag{2.32}$$

This yields

$$72NQ_{xx}Q_{xy}[2 + N(-1 + 4Q_{xx}^2 - 8Q_{xx}Q_{xy} + 12Q_{xy}^2)] = 0. \tag{2.33}$$

Solving these three equations in a neighborhood of $N = 2$, $Pe = 0$, we obtain the 2D scaling behavior

$$Pe \simeq \frac{2}{a\sqrt{3}}[\frac{(N-2)^3}{N}]^{1/2}. \tag{2.34}$$

This behavior is quite different from the analogous 3D result (Forest *et al.*, 2004; See *et al.*, 1990). In Fig. 2.3, this 2D scaling prediction is compared with eleven (11) bifurcation diagrams for fixed finite values $0 < Pe < 0.02$, employing the continuation software AUTO. One such representative bifurcation diagram is given in Fig. 2.5 for $Pe = 0.1$; the data point labeled LP2 is the object of the formula (2.34) and provides one data point in Fig. 2.3.

2.4.3 The nematic equilibrium branch

We parameterize the S^1 invariant director $\mathbf{m}_0$ by $\mathbf{m}_0 = (\cos\theta, \sin\theta)$. As explained earlier, the unique nematic equilibrium branch has order parameter $s_+ = \sqrt{1 - \frac{2}{N}}$. Therefore

the nematic equilibrium has an explicit representation:

$$\mathbf{Q}_0 = s_+(\mathbf{m}_0\mathbf{m}_0 - \frac{\mathbf{I}}{2}) = \frac{s_+}{2}\begin{pmatrix} \cos 2\theta & \sin 2\theta \\ \sin 2\theta & -\cos 2\theta \end{pmatrix}. \tag{2.35}$$

The solvability equation (2.21) has the following ingredients for the nematic phase:

$$\mathbf{A}_1 = \frac{6s_+^2}{1-s_+^2}\begin{pmatrix} 1+\cos 4\theta & \sin 4\theta \\ \sin 4\theta & 2\sin^2 2\theta \end{pmatrix}, \tag{2.36}$$

$$\mathbf{r}_1 = \begin{pmatrix} \frac{1}{2}s_+(1-as_+\cos 2\theta)\sin 2\theta, \\ -\frac{1}{2}s_+\cos 2\theta + \frac{a}{4}(2-s_+^2(1-\cos 4\theta)) \end{pmatrix}. \tag{2.37}$$

The eigenvalues of the system are:

$$-\frac{Pe}{2}(4-4s_+^2+3as_+\cos 2\theta)\tan 2\theta, \quad -\frac{12s_+^2}{1-s_+^2} + O(Pe) \tag{2.38}$$

with corresponding vectors

$$v_1 = (-\tan 2\theta, 1), \ v_2 = (\cot 2\theta, 1). \tag{2.39}$$

If $N > 2$, the eigenvector v_1 spans the null space of $\mathbf{A}_1^T$, so the solvability condition simplifies to $\mathbf{r}_1^T v_1 = 0$. After simplification, we get $\mathbf{r}_1^T v_1 = \frac{1}{2}(a - s\sec 2\theta)$, which produces the Leslie alignment angle in weak shear for the Doi closure

$$\cos 2\theta = \frac{s_+}{a} = \frac{1}{a}\sqrt{1-\frac{2}{N}} \equiv 1/\lambda_L, \tag{2.40}$$

where λ_L is the Leslie alignment parameter mentioned in Section 2.3. For $|\lambda_L| < 1$, any solution that exists must be unsteady. If $|\lambda_L| > 1$, the equation (2.40) has two distinct

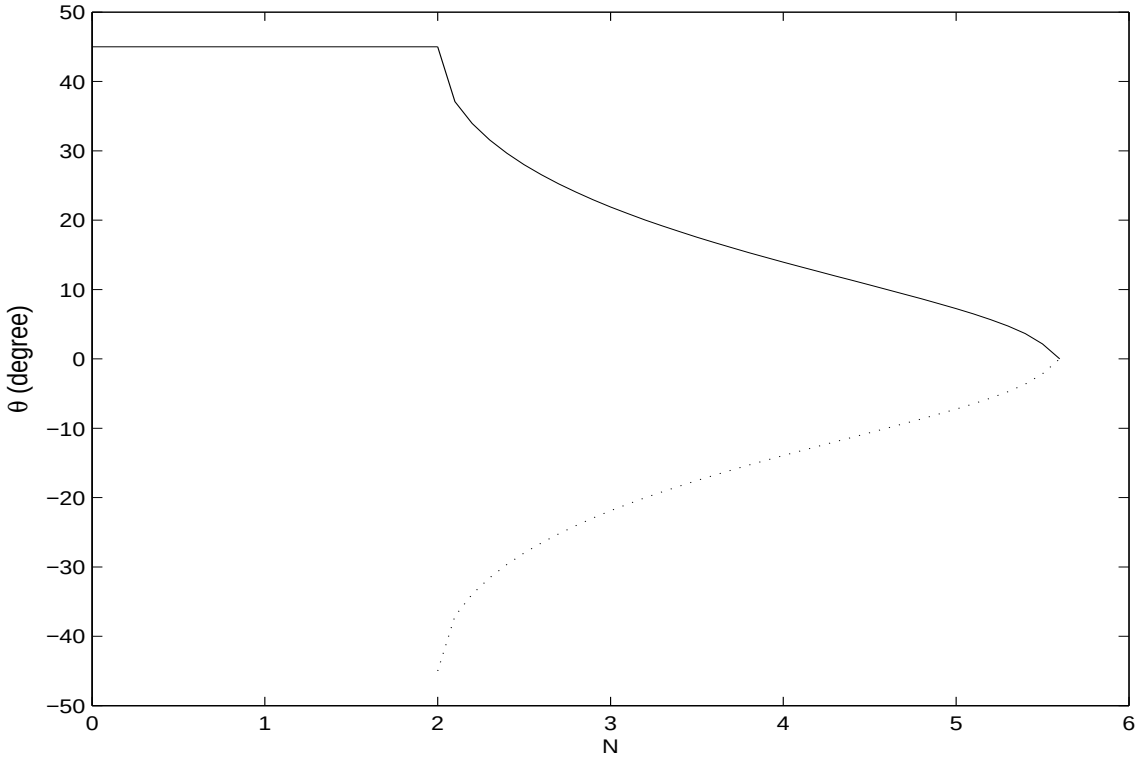

Figure 2.4: The steady state Leslie alignment angle θ, formula (2.40), plotted versus nematic concentration N for aspect ratio $r = 3$. The solid (dotted) lines represent stable (unstable) solutions.

steady solutions (one stable and one unstable),

$$\theta = \frac{1}{2} \arccos \frac{s_+}{a}, \tag{2.41}$$

for $-\frac{\pi}{2} < \theta < \frac{\pi}{2}$. From (2.38) and (2.40), the solution is stable if $-\frac{\pi}{2} < \theta < -\frac{\pi}{4}$ when a is negative (i.e. disk-like molecules) or $0 < \theta < \frac{\pi}{4}$ when a is positive (i.e. rod-like molecules). Otherwise, the solution is unstable. This yields agreement with Fig. 2.5 predicting the upper two (solid and dotted) curves between LP1 and LP2.

We solve the linear system (2.21) as well as the next order system (2.27), which yields:

$$\mathbf{Q} = \mathbf{Q}_0 + Pe \frac{(1 - s_+^2)^2}{12 s_+} \begin{pmatrix} 2 \sin 2\theta & -\cos 4\theta \sec 2\theta \\ -\cos 4\theta \sec 2\theta & -2 \sin 2\theta \end{pmatrix} + O(Pe^2). \tag{2.42}$$

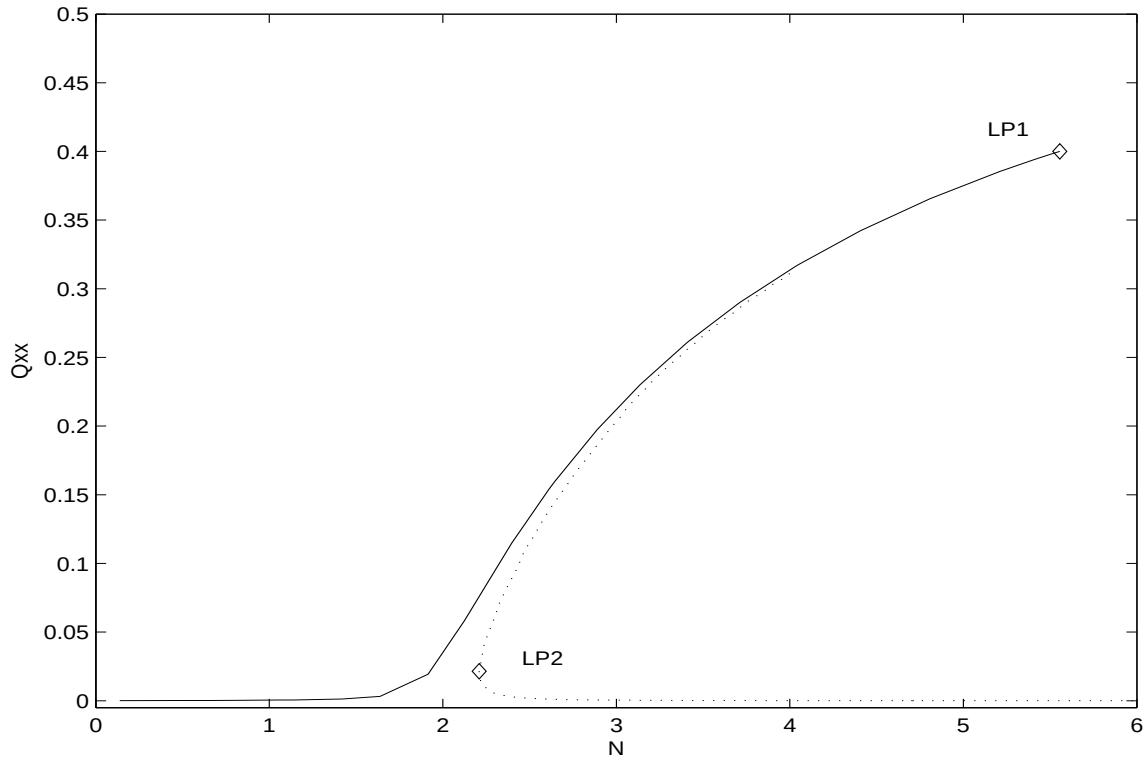

Figure 2.5: Steady state solution branches of the Doi closure model are plotted for $Pe = 0.1$ using AUTO. Two folds exist at N=2.21 and 5.556. The unsteady regime starts at N=5.556.

- For infinite aspect ratio $|a| = 1$, the right hand side of (2.40) always has modulus less than 1, i.e. $\mathbf{Q}_1$ is solvable.

- For $|a| < 1$, the right hand side of (2.40) will hit values ± 1 at a critical concentration N. The relationship between this critical concentration and the aspect ratio r is discovered as

$$N_*(a) = \frac{2}{1-a^2} = \frac{1}{2}\left(r + \frac{1}{r}\right)^2. \tag{2.43}$$

  - For $2 < N \leq N_*(a)$, $\mathbf{Q}_1$ is solvable, i.e. steady solutions exist.
  - For $N > N_*(a)$, no steady solution exists for $\mathbf{Q}_1$.

$N_*(a)$ predicts the AUTO generated bifurcation LP1, which represents the termination of a steady state solution branch. For $r = 3$ or $r = 1/3$, $N_*(a) = N_*(\pm 0.8) \approx 5.556$, which yields the point LP1 in Fig. 2.5. Marrucci and Maffettone (Marrucci and Maffetone,

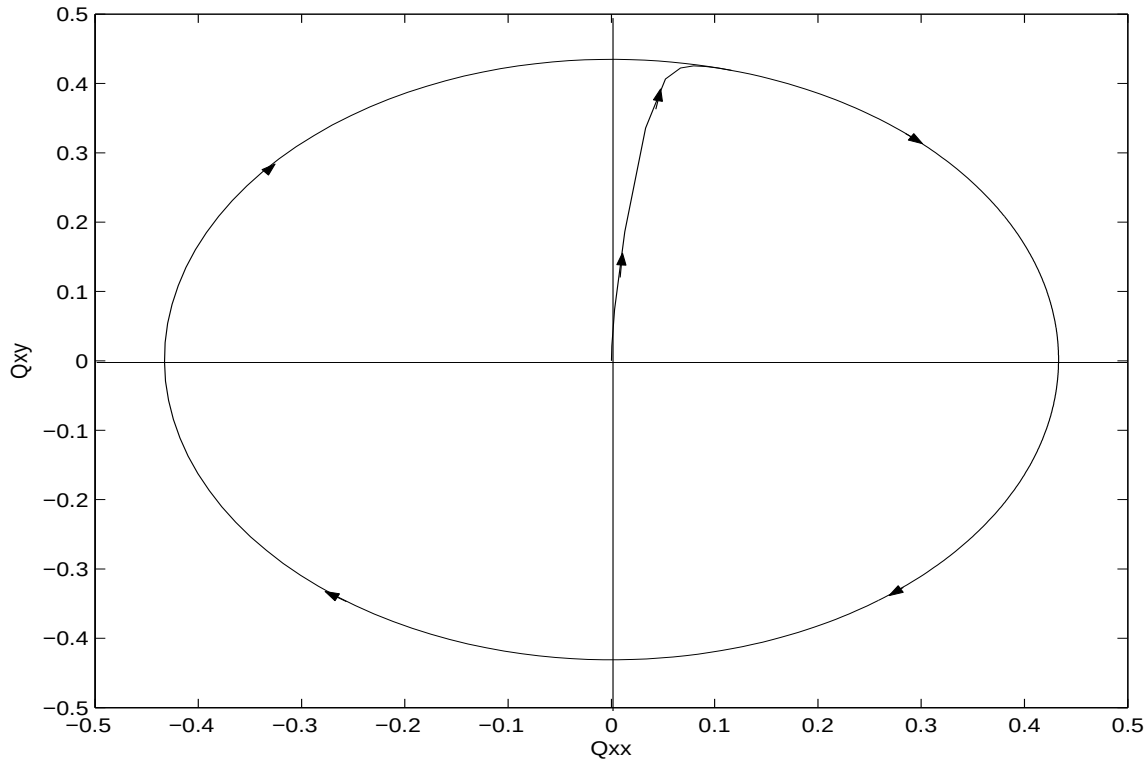

Figure 2.6: Convergence of a sample orbit to the tumbling limit cycle for N=8, Pe=0.66, a=0.8, in the Doi closure model.

1989) predicted $N_*(a) = 2.41$ for the rigid rod ($a = 1$) kinetic model, but the meaning of parameters N and a is blurred in the projection onto second moment models.

2.5 Limit cycles in unsteady regimes

The next task is to characterize oscillatory solutions at the onset of simple shear, beyond the statement that they are expected since $|\lambda_L(a, N)| < 1$ in formula (2.40).

Theorem 2.5.1 *For sufficiently small $Pe \neq 0$ and $N > N_*(a) = \dfrac{2}{1-a^2}$, there exists a stable limit cycle of* (2.13)*, equivalently* (2.17)*.*

Proof. The Poincaré-Bendixson Theorem states that in a closed, bounded subset R of the plane, if R has no fixed points and there exists a trajectory C that is confined in R, then R contains a closed orbit, i.e. a limit cycle. To be sure that a confined trajectory

C exists, we will show there is a trapping region R, i.e. a closed connected set such that the vector field points inward everywhere on the boundary of R.

If $N > \dfrac{2}{1-a^2}$, then the Leslie parameter λ_L obeys $|\lambda_L| < 1$. From (2.17), $\dot{\theta}$ can never be zero. Thus there is no fixed point. Since $-1 \leq a(1-s^2)\sin 2\theta \leq 1$,

$$-3s[N(s^2-1)+2] - Pe \leq \dot{s} \leq -3s[N(s^2-1)+2] + Pe.$$

For sufficiently small Pe, we can assume $\dot{s} \approx -3s[N(s^2-1)+2]$. If we choose $s_{max}^2 = 1 + \varepsilon_1 - \dfrac{2}{N}$, where $0 < \varepsilon_1 < \frac{2}{N}$, then $\dot{s}_{max} \approx -3s_{max}(\varepsilon_1 N) < 0$. If we choose $s_{min}^2 = 1 - \varepsilon_2 - \dfrac{2}{N}$, where $0 < \varepsilon_2 < 1 - \frac{2}{N}$, then $\dot{s}_{min} \approx 3s_{min}(\varepsilon_2 N) > 0$. Hence by the Poincaré-Bendixson Theorem, there exists a closed orbit. $\square$

To characterize the bifurcation N_* following (Vicente *et al.*, 2003), we expand the equation (2.17) using the method of two time scales as $Pe \to 0$; the fast $O(1)$ time scale $T_0 = t$ and slow time scale $T_1 = Pe \cdot t$. Then the expansions are

$$s = s_0(T_0, T_1) + Pe \cdot s_1(T_0, T_1) + O(Pe^2) \tag{2.44}$$

$$\theta = \theta_0(T_0, T_1) + Pe \cdot \theta_1(T_0, T_1) + O(Pe^2). \tag{2.45}$$

At leading order, the equations give $s_0 = s_+ = \sqrt{1 - \frac{2}{N}}$, $\partial\theta_0/\partial T_0 = 0$ and so $\theta_0(T_0, T_1) = \Theta_0(T_1)$. At first order in Pe,

$$\theta_1 = -T_0[\frac{d\Theta_0}{dT_1} + \frac{1}{2}(1 - \frac{a}{s_0}\cos 2\Theta_0)] + C(T_1), \tag{2.46}$$

where $C(T_1)$ is a function of T_1 alone. To make θ_1 independent of T_0,

$$\frac{d\Theta_0}{dT_1} + \frac{1}{2}(1 - \frac{a}{s_0}\cos 2\Theta_0) = 0. \tag{2.47}$$

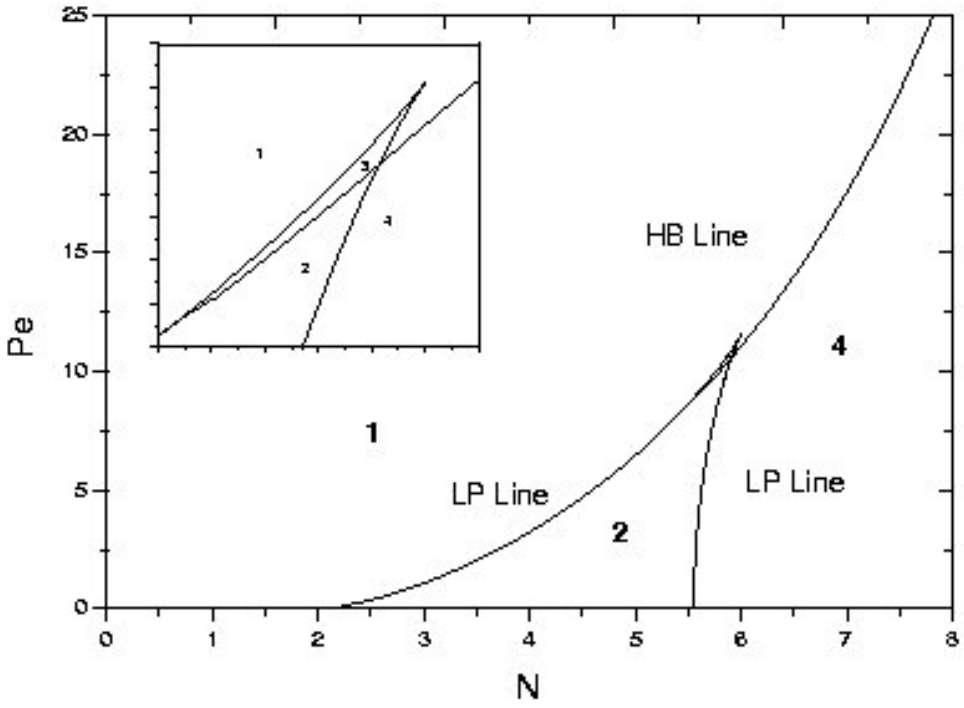

Figure 2.7: N-Pe phase diagram of the 2D Doi closure model. The parameter space is divided into 4 regions. The Regions 1, 2, 3 are governed by flow-aligning states whereas Region 4 has tumbling or wagging, stable limit cycles.

So, the period of the periodic orbit is

$$T = \frac{4\pi s_0}{Pe\sqrt{s_0^2 - a^2}}. \tag{2.48}$$

This shows that the period of the limit cycle is infinite as s_0 goes to a. Since $s_0 = \sqrt{1 - \frac{2}{N}}$ for $Pe \ll 1$, the period goes to infinity as $N \to N_*(a) = \frac{2}{1-a^2}$, as confirmed by AUTO in Fig. 2.7 by passing from Region 4 into Region 2.

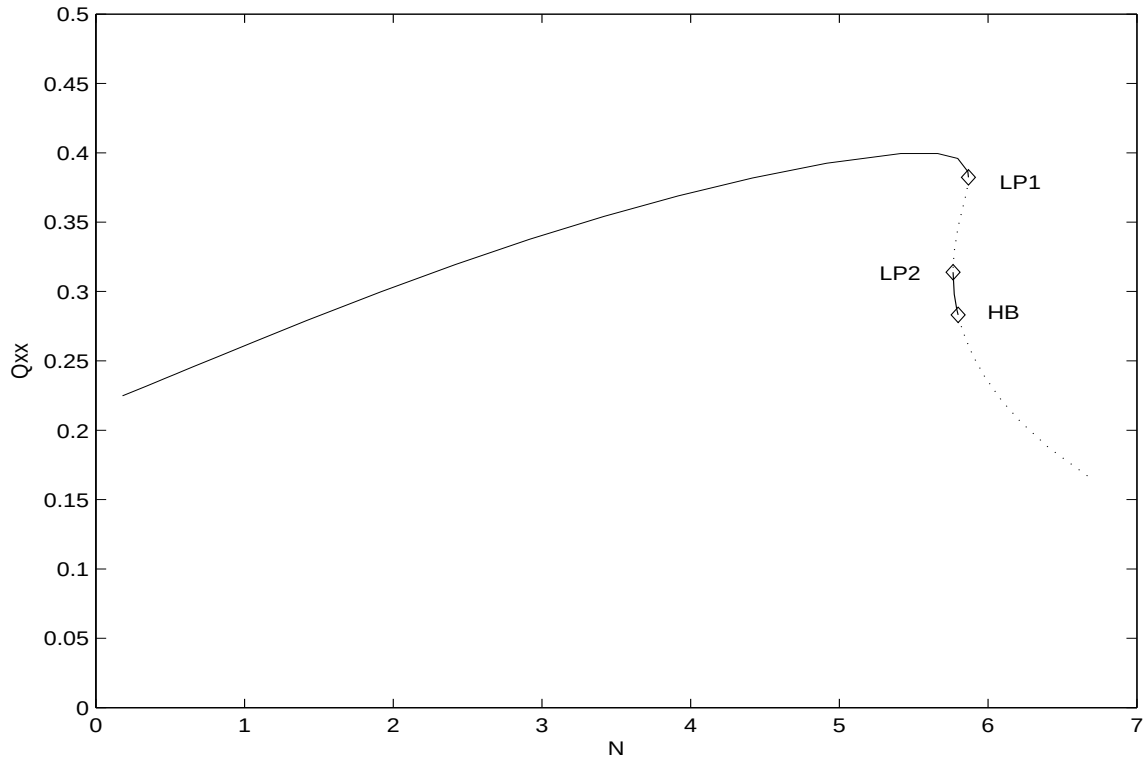

Figure 2.8: The steady state solutions of the Doi closure model for $Pe = 10$.

2.6 The phase diagram of mesoscopic models: Robustness vs sensitivity to closure

In this section we summarize the behavior of a liquid crystal polymer monolayer in shear flow in terms of phase diagrams. We calculate steady state solutions and bifurcation branches, using XPPAUT and AUTO 97 for several closure models. The aspect ratio parameter is fixed as $a = 0.8$ in each model.

Fig. 2.7 is the phase diagram for the Doi closure in (N, Pe)-space. This figure shows that Hopf bifurcation ends at a limit point LP2. Vicente Alonso showed this point is a so-called Bogdanov-Takens bifurcation in a 3D Landau-de Gennes model (Vicente *et al.*, 2003). The parameter space is separated into 4 regions:

Region 1 There is only one stable steady state solution, the perturbed isotropic phase.

Region 2 There are one stable and two unstable states (Fig. 2.5).

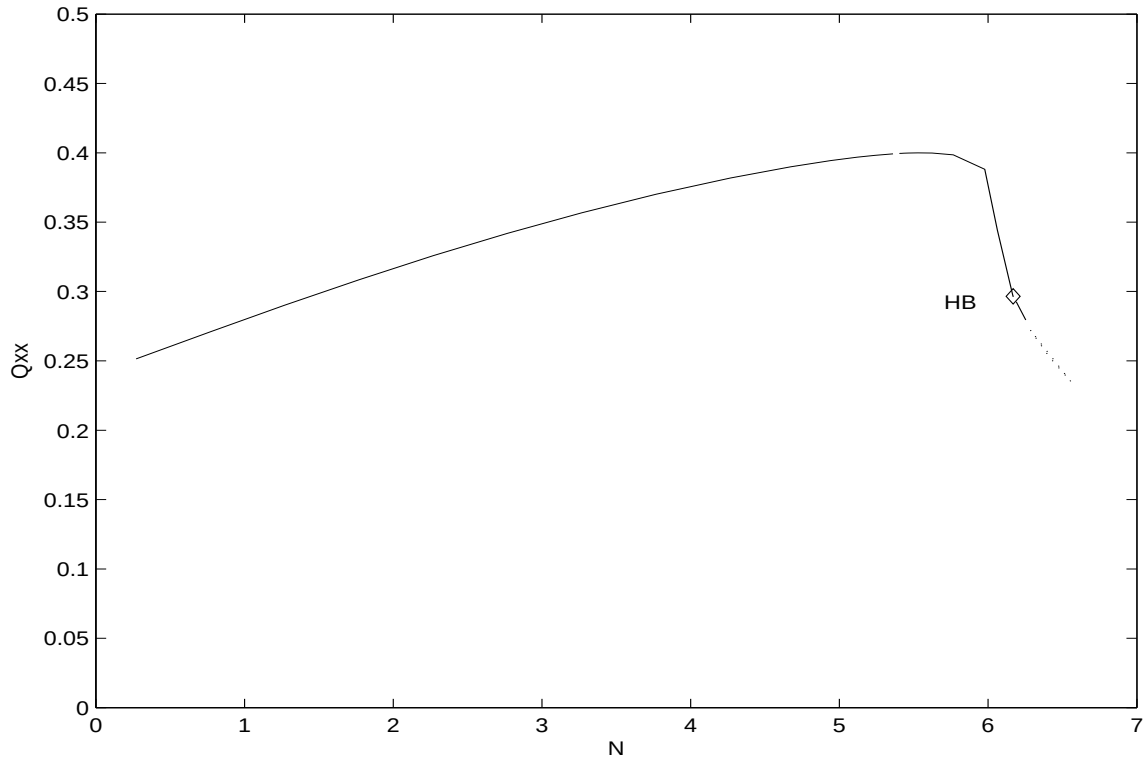

Figure 2.9: The steady state solution of the Doi closre model for $Pe = 12$.

Region 3 There are two stable steady states. The nematic steady state is destabilized by the Hopf bifurcation (Fig. 2.8).

Region 4 There is one unstable steady state and a stable limit cycle. The limit cycle is generated by a global bifurcation called a saddle homoclinic bifurcation until $O(Pe) \sim 1$. For larger values of Pe, the limit cycle emanates from a Hopf bifurcation (Fig. 2.9).

The bifurcation diagram for the Doi model and that of the Hinch-Leal 1 model, Fig. 2.10, are able to capture the Bogdanov-Takens bifurcation (Vicente *et al.*, 2003) which is faithful to the 2D kinetic phase diagram (Maffetone and Crescitelli, 1995). Fig. 2.10 and Fig. 2.11 show the Hinch-Leal and Tsuji-Rey closures compress Region 3 so that detection of this aspect of the dynamical system is extremely sensitive to numerical error.

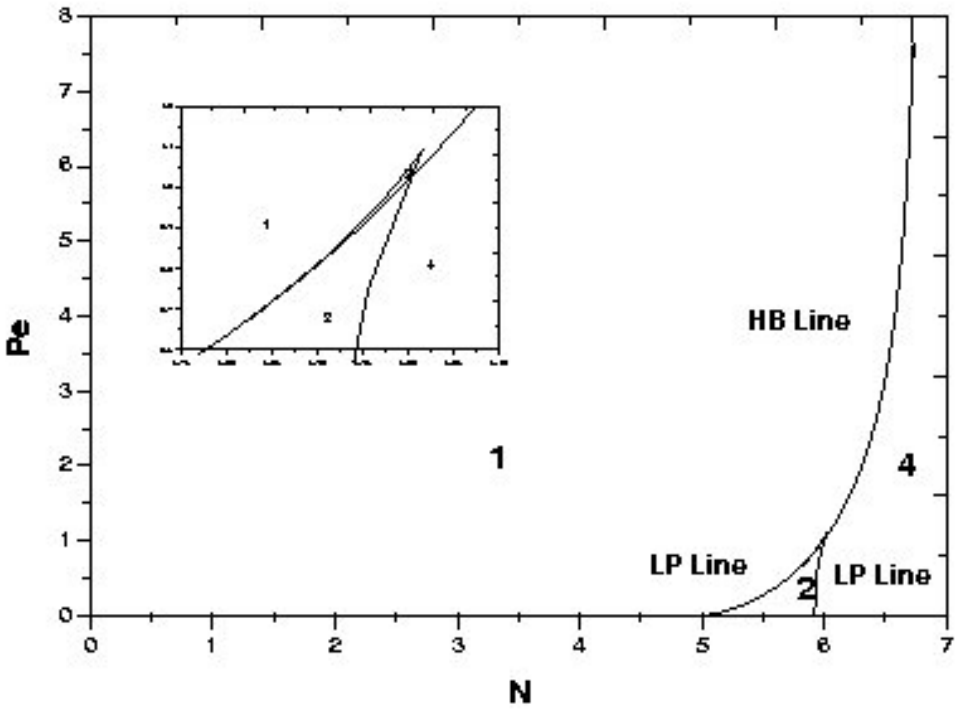

Figure 2.10: *N-Pe* Phase diagram for the Hinch-Leal 1 model. The 4 regions are same as the Doi model.

2.7 Conclusion

In this chapter, we derived weak-shear steady and unsteady selection criteria for two-dimensional nematic polymers using various second-moment closures. These results are valid except in a neighborhood of the isotropic-nematic transition at $N = 2$; the persistence of this bifurcation point for low Pe is deduced by methods similar to See *et al.* (See *et al.*, 1990) and Forest *et al.* (Forest *et al.*, 2004) for three-dimensional nematic liquids. The analysis is then confirmed with numerical simulations using the continuation software AUTO. We showed the existence of a limit cycle beyond the parameter boundary for the steady-unsteady transition as an application of the Poincaré-Bendixon Theorem and characterized the transition boundary in the phase diagram in the weak shear limit. The shear-perturbed 2D phase diagrams for the three closure models (Doi, Tsuji-Rey and Hinch-Leal 1) are remarkably robust relative to the 3D shear problem.

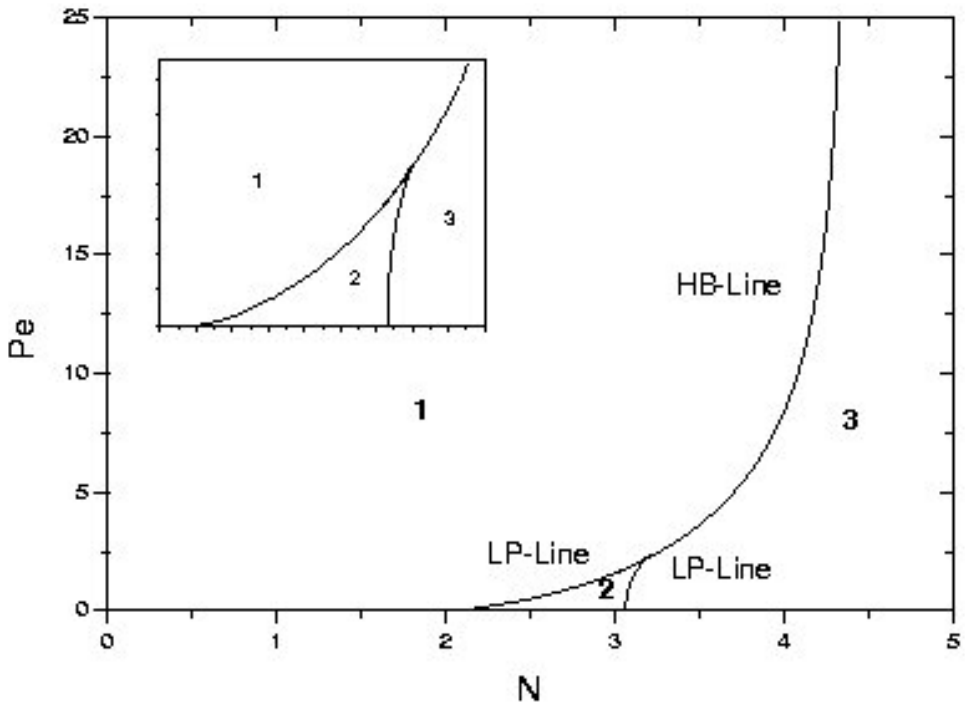

Figure 2.11: N-Pe Phase diagram of the Tsuji-Rey model. The aspect parameter ratio a is fixed at 0.8. Regions 1,2 consist of flow-aligning states while Region 3 has tumbling-wagging limit cycles.

Chapter 3

Analysis of a 2D Smoluchowski equation for flowing magnetic dispersions

3.1 Introduction

Many liquid crystalline substances are composed of molecules with a permanent dipole moment. In (Bhandar and Wiest, 2003), Bhandar and Wiest extended the Doi-Hess model for rigid rod-like nematic polymers to dipolar nano-rod dispersions. They developed the model including magnetic effects, e.g. the effects of external magnetic fields and the magnetic interactions that exist between the permanent magnetic moments in the ferromagnetic rods. This simple kinetic model gives rise to a Smoluchowski equation for the orientational probability distribution function (PDF). Recently, various attempts have been made to solve the Smoluchowski equation analytically or numerically (Constantin *et al.*, 2004; Forest *et al.*, 2007; Ji *et al.*, 2007; Wang *et al.*, 2005; Zarnescu, 2006). In this model, the fore-aft symmetry of the PDF is broken due to magnetic polarity of the particle. Thus the first moment of the PDF, which is zero for non-ferromagnetic particles, strongly couples to the second moment. The dynamics of magnetic dispersions were studied using moment closure equations in (Bhandar and Wiest, 2003; Grandner *et al.*, 2007).

In this chapter, we extend the previous work. We obtain the exact steady state solution of the Smoluchowski equation under general linear flows in semi-implicit form. Steady state solutions of the Smoluchowski equation under imposed magnetic fields and linear flow fields with zero vorticity tensor are of Boltzmann type, and therefore completely determined by the total potential (Constantin *et al.*, 2004; Wang *et al.*, 2005). The total potential can be parameterized by order parameters and material parameters, and governed by algebraic-integral equations. Even though these equations are transcendental, they represent an exact, finite-dimensional reduction of the infinite-dimensional PDE. We focus on the equation with dipolar and Maier-Saupe interaction potentials and no external fields. We construct bifurcation diagrams by solving the algebraic-integral equations and investigating the stability of solutions in terms of the free energy functional.

3.2 Steady state solutions under an imposed general linear flow and magnetic field

Let $\mathbf{m}$ be a unit vector for the axis of symmetry of the molecule and $f(\mathbf{m}, t)$ be the orientational probability distribution function (PDF). Average properties are defined in terms of this PDF as $< \mathbf{m} >= \int \mathbf{m} f(\mathbf{m}, t) d\mathbf{m}$, $< \mathbf{mm} >= \int \mathbf{mm} f(\mathbf{m}, t) d\mathbf{m}$. In the presence of an external magnetic field $\mathbf{H}$, the total potential is given by

$$V_t(\mathbf{m}) = -k_B T[\alpha \mathbf{m} \cdot < \mathbf{m} > + \nu \mathbf{m} \cdot \mathbf{H} + 2N < \mathbf{mm} > : \mathbf{mm} + \frac{\alpha_0}{2} \mathbf{HH} : \mathbf{mm}], \quad (3.1)$$

where α is the strength of dipolar interaction, ν is the strength of the permanent dipole, N is the concentration and α_0 is the difference between the susceptibility parallel and perpendicular to the molecular direction. The first term of (3.1) is the dipole-dipole interaction potential. The second term is the interaction with the external magnetic field and the third term is the Maier-Saupe interaction potential. When an external magnetic

field is imposed, an induced moment occurs yielding the last term.

The rotational transport equation for the PDF is given by

$$\frac{\partial}{\partial t}f = D_r^0 \frac{\partial}{\partial \mathbf{m}} \cdot (f \frac{\partial \mu}{\partial \mathbf{m}}) - \frac{\partial}{\partial \mathbf{m}} \cdot (\dot{\mathbf{m}} f), \tag{3.2}$$

$$\dot{\mathbf{m}} = \mathbf{\Omega} \cdot \mathbf{m} - a[\mathbf{D} \cdot \mathbf{m} + \mathbf{D} : \mathbf{mmm}], \tag{3.3}$$

$$\mu = \ln f + \frac{1}{k_B T} V_t, \tag{3.4}$$

where D_r^0 is an averaged relaxation rate, $\frac{\partial}{\partial \mathbf{m}} = (\mathbf{I} - \mathbf{mm}) \cdot \bigtriangledown_{\mathbf{m}}$ is the rotational gradient operator, $\mathbf{D}$ and $\mathbf{\Omega}$ are the rate-of-strain tensor and vorticity tensor, respectively, a is the molecular shape parameter related to the molecular aspect ratio r as $a = \frac{r^2-1}{r^2+1}$, and μ is the normalized chemical potential.

We assume a homogeneous flow i.e.

$$\nabla v = \begin{pmatrix} v_{11} & v_{12} \\ v_{21} & -v_{11} \end{pmatrix} \tag{3.5}$$

where v_{ij} are constant.

The rate of strain tensor $\mathbf{D}$ and the vorticity tensor $\mathbf{\Omega}$ are defined as

$$\mathbf{D} = \frac{1}{2}(\nabla v + \nabla v^T) = \begin{pmatrix} v_{11} & p \\ p & -v_{11} \end{pmatrix}, \tag{3.6}$$

$$\mathbf{\Omega} = \frac{1}{2}(\nabla v - \nabla v^T) = q \begin{pmatrix} 0 & 1 \\ -1 & 0 \end{pmatrix} \tag{3.7}$$

where $p = \frac{v_{12}+v_{21}}{2}$ and $q = \frac{v_{12}-v_{21}}{2}$.

Since $\mathbf{D}$ is symmetric and constant,

$$\begin{aligned}\frac{\partial}{\partial \mathbf{m}} \cdot (\mathbf{D} : \mathbf{mm}) &= (\mathbf{I} - \mathbf{mm}) \cdot \bigtriangledown_{\mathbf{m}} (\mathbf{D} : \mathbf{mm}) \\ &= (\mathbf{I} - \mathbf{mm}) \cdot (\mathbf{D} : (\mathbf{Im} + \mathbf{mI})) \\ &= \mathbf{D} \cdot \mathbf{m} - \mathbf{D} : \mathbf{mmm}. \end{aligned} \tag{3.8}$$

Therefore the straining component can be absorbed into an effective chemical potential $\tilde{\mu}$ as follows:

$$\frac{\partial}{\partial t} f = \frac{\partial}{\partial \mathbf{m}} \cdot (D_r f \frac{\partial \tilde{\mu}}{\partial \mathbf{m}}) - \frac{\partial}{\partial \mathbf{m}} \cdot (\mathbf{\Omega} \cdot \mathbf{m} f), \tag{3.9}$$

$$\tilde{\mu} = \mu + \frac{1}{k_B T} V_{\mathbf{D}}, \tag{3.10}$$

$$V_{\mathbf{D}} = \frac{a k_B T}{D_r} \mathbf{D} : \mathbf{mm}. \tag{3.11}$$

One observes that the straining flow field potential is equivalent to the magnetic field potential term, $V_{\mathbf{H}} = -\frac{\alpha_0 k_B T}{2} \mathbf{HH} : \mathbf{mm}$. The straining flow modifies the magnetic field strength $V_{\mathbf{H}}$,

$$V^{eff} = V_{\mathbf{H}} + \frac{1}{k_B T} V_{\mathbf{D}} = (-\frac{\alpha_0 k_B T}{2} \mathbf{HH} + \frac{a}{Dr} \mathbf{D}) : \mathbf{mm}. \tag{3.12}$$

Thus, key issue remaining here is rotational flow term. Let $\mathbf{m} = (\cos\theta, \sin\theta)$ and $\mathbf{t}$ be an orthogonal vector such that $\mathbf{t} = (-\sin\theta, \cos\theta)$, then $\frac{\partial}{\partial \mathbf{m}} = \mathbf{t} \frac{\partial}{\partial \theta}$. The Smoluchowski equation (3.9) is

$$\begin{aligned}\frac{\partial f}{\partial t} &= \mathbf{t} \frac{\partial}{\partial \theta} \cdot (D_r f \mathbf{t} \frac{\partial \tilde{\mu}}{\partial \theta}) - \mathbf{t} \frac{\partial}{\partial \theta} \cdot (\mathbf{\Omega} \cdot \mathbf{m} f) \\ &= \frac{\partial}{\partial \theta} (D_r f \frac{\partial \tilde{\mu}}{\partial \theta}) - \mathbf{t} \frac{\partial}{\partial \theta} \cdot (\mathbf{\Omega} \cdot \mathbf{m} f). \end{aligned} \tag{3.13}$$

Since

$$\begin{aligned} \mathbf{\Omega}\cdot\mathbf{m} &= q\begin{pmatrix} 0 & 1 \\ -1 & 0 \end{pmatrix}\begin{pmatrix} \cos\theta \\ \sin\theta \end{pmatrix} = q\begin{pmatrix} \sin\theta \\ -\cos\theta \end{pmatrix} \\ &= -q\mathbf{t} = -\mathbf{t}\tfrac{\partial}{\partial\theta}(q\theta + q_0), \end{aligned} \tag{3.14}$$

the 2D reduction of the vorticity contribution is again a grad flow (Zarnescu, 2006) and we can absorb the vorticity component in the extended chemical potential $\bar{\mu}$.

$$\frac{\partial f}{\partial t} = \frac{\partial}{\partial\theta}(D_r f\frac{\partial\bar{\mu}}{\partial\theta}), \tag{3.15}$$

$$\bar{\mu} = \mu + \frac{1}{k_B T}(V_{\mathbf{D}} + V_{\mathbf{\Omega}}), \tag{3.16}$$

$$V_{\mathbf{\Omega}} = -\frac{k_B T}{D_r}(q\theta + q_0). \tag{3.17}$$

The steady state solution of the equation (3.15)

$$D_r f\cdot\frac{\partial\bar{\mu}}{\partial\theta} = D_r(\frac{\partial f}{\partial\theta} + f\frac{\partial}{\partial\theta}V) = C_1 \tag{3.18}$$

leads to

$$f(\theta) = f(\theta_0)e^{V(\theta_0)-V(\theta)} + C\int_{\theta_0}^{\theta} e^{V(\sigma)-V(\theta)}d\sigma, \tag{3.19}$$

$$V = \frac{1}{k_B T}[V_t + V_{\mathbf{D}} + V_{\mathbf{\Omega}}]. \tag{3.20}$$

The integration constant C plays a critical role (Zarnescu, 2006) in restoring 2π-periodicity of f, with the result

$$C = \frac{f(0)(1-e^{-2q\pi})}{\int_0^{2\pi} e^{V(\sigma)-V(2\pi)}d\sigma}. \tag{3.21}$$

If the vorticity tensor $\mathbf{\Omega}$ is zero, i.e. $q = 0$, steady state solutions are of Bltzmann type.

3.3 Equilibrium case

We consider the case that external flow and magnetic field effects are absent. So, the total potential (3.20) reduces to

$$V(\mathbf{m}) = -[\alpha \mathbf{m}\cdot < \mathbf{m} > +2N < \mathbf{mm} >: \mathbf{mm}]. \tag{3.22}$$

Then the steady state solution is given by a Boltzmann distribution

$$f = \frac{1}{Z} e^{-V} \tag{3.23}$$

where Z is the normalizing coefficient. Let $\mathbf{n}_1$, $\mathbf{n}_2$ be the two orthonormal eigenvectors of the second moment tensor $< \mathbf{mm} >$. Then the unit vector $\mathbf{m}$ and the first moment $< \mathbf{m} >$ are parameterized as

$$\begin{aligned} \mathbf{m} &= \cos\theta \mathbf{n}_1 + \sin\theta \mathbf{n}_2 \\ < \mathbf{m} > &= s_1[\cos\theta' \mathbf{n}_1 + \sin\theta' \mathbf{n}_2], \end{aligned} \tag{3.24}$$

where s_1 is a *polar order parameter* which measures the average polarity in the dispersion. The second moment can be represented by the director $\mathbf{n}_1$ and the order parameter s as we have already seen in Chapter 2:

$$< \mathbf{mm} >= s(\mathbf{n}_1\mathbf{n}_1 - \frac{1}{2}\mathbf{I}) + \frac{1}{2}\mathbf{I}. \tag{3.25}$$

With the above parametrization, the order parameters are given by

$$\begin{aligned} s_1 &= \frac{1}{s_1} < \mathbf{m} > \cdot < \mathbf{m} >= \frac{1}{s_1} << \mathbf{m} > \cdot \mathbf{m} > \\ &= < \cos\theta\cos\theta' + \sin\theta\sin\theta' > \end{aligned} \tag{3.26}$$

$$s = 2\mathbf{n}_1\cdot < \mathbf{mm} > \cdot\mathbf{n}_1 - 1 = 2 < (\mathbf{n}_1 \cdot \mathbf{m})^2 > -1 =< \cos 2\theta > \tag{3.27}$$

where the averages are defined in terms of the equilibrium PDF

$$f = \frac{1}{Z} e^{\alpha s_1(\cos\theta\cos\theta' + \sin\theta\sin\theta') + N(s\cos 2\theta + 1)}. \tag{3.28}$$

In the equilibrium case, the first moment is in the eigenspace of the second moment. The relation and the proof established in (Ji *et al.*, 2007) for 3D pass to 2D as follows.

Theorem 3.3.1 *The first moment vector either vanishes or must be parallel to one of the eigenvectors of the second moment tensor.*

Proof. We want to prove that $< \mathbf{m} >$ is parallel to one of the eigenvectors of the second moment $< \mathbf{mm} >$. Without loss of generality, we can choose x and y axes such that the second moment tensor is diagonal i.e. $< m_1 m_2 >= 0$. Let $\mathbf{e}_1$ and $\mathbf{e}_2$ be the orthonormal basis of the eigenspace. Now expand $< \mathbf{m} >$ in the basis, $< \mathbf{m} >= r_1\mathbf{e}_1 + r_2\mathbf{e}_2$ and we want to show that r_1 or r_2 is zero. The total potential is

$$\begin{aligned} \frac{V(m_1, m_2)}{k_B T} &= -\alpha(r_1 m_1 + r_2 m_2) - (c_1 m_1^2 + c_2 m_2^2) \\ &= -\alpha(r_1 m_1 + r_2 m_2) - B(m_1, m_2), \end{aligned} \tag{3.29}$$

where $c_j = 2N < m_j m_j >$. Note that B is an even function of m_1 and m_2.

$$\begin{aligned} < m_1 m_2 > &= \frac{1}{Z} \int_{|\mathbf{m}|=1} m_1 m_2 \exp[r_1 m_1 + r_2 m_2 + B(m_1, m_2)] d\mathbf{m} \\ &= \frac{1}{Z} \int_{|\mathbf{m}|=1 \text{ with } m_1>0, m_2>0} m_1 m_2 \exp[B(m_1, m_2)] \times \\ &\quad [\exp(r_1 m_1 + r_2 m_2) - \exp(-r_1 m_1 + r_2 m_2) \\ &\quad - \exp(r_1 m_1 - r_2 m_2) + \exp(-r_1 m_1 - r_2 m_2)] d\mathbf{m} \\ &= \frac{4}{Z} \int_{|\mathbf{m}|=1 \text{ with } m_1>0, m_2>0} m_1 m_2 e^{B(m_1, m_2)} \times \\ &\quad \sinh(r_1 m_1) \sinh(r_2 m_2) d\mathbf{m}. \end{aligned} \tag{3.30}$$

Since $\sinh(x)$ is zero if and only if $x = 0$, r_1 or r_2 should be zero in order to make the

integration zero. Hence $< \mathbf{m} >$ is either parallel to $\mathbf{e_1}$ or $\mathbf{e_2}$. $\square$

Now let's assume that $< \mathbf{m} >$ is parallel to $\mathbf{n}_1$, i.e. $\theta' = 0$. From (3.26) to (3.28), s_1 and s are determined by solving the system of algebraic equations

$$\int_0^{2\pi} (s_1 - \cos\theta) e^{\alpha s_1 \cos\theta + Ns\cos 2\theta} d\theta = 0 \tag{3.31}$$

$$\int_0^{2\pi} (s - \cos 2\theta) e^{\alpha s_1 \cos\theta + Ns\cos 2\theta} d\theta = 0. \tag{3.32}$$

We note that for any α and N, $s_1 = 0$ is a solution corresponding to the purely nematic solution branch which is already well known. Also, $< \mathbf{m} >= s_1(\cos\theta', \sin\theta') = -s_1(\cos(\theta'+\pi), \sin(\theta'+\pi))$ implies that $-s_1$ is equivalent to s_1. Hence, we will consider only positive s_1 here.

In (Ji *et al.*, 2007), the authors establish a lower bound on the material parameter α below which solutions are purely nematic for the 3D model. We now obtain the identical lower bound on α for the 2D model following their method.

Theorem 3.3.2 *There exist only purely nematic equilibria* ($s_1 = 0$) *when* $\alpha \leq 1$.

Proof. Since $< \mathbf{m} >$ is parallel to $\mathbf{n}_1$, $< \mathbf{m} >$ can be rewritten as $< \mathbf{m} >= r_1\mathbf{e}_1$. We will show that when $\alpha \leq 1$, r_1 must be zero so the only equilibrium is non-polar. We prove it by contradiction. Suppose $r_1 > 0$, otherwise we can change the coordinate system to achieve this.

$$\begin{aligned} r_1 =< m_1 > &= \frac{\int m_1 \exp[\alpha r_1 m_1 + B(m_1, m_2)]}{\int \exp[\alpha r_1 m_1 + B(m_1, m_2)]} \\ &= \frac{\int_{m_1>0} m_1 \exp[B(m_1, m_2)] \sinh(\alpha r_1 m_1)}{\int_{m_1>0} \exp[B(m_1, m_2)] \cosh(\alpha r_1 m_1)}. \end{aligned} \tag{3.33}$$

Using the fact that $\tanh x < x$ for $x > 0$, we have

$$\begin{aligned} & m_1 \exp[B(m_1, m_2)] \sinh(\alpha r_1 m_1) \\ \leq & \exp[B(m_1, m_2)] \cosh(\alpha r_1 m_1) \tanh(\alpha r_1 m_1) \\ < & \alpha r_1 \exp[B(m_1, m_2)] \cosh(\alpha r_1 m_1). \end{aligned} \tag{3.34}$$

Substituting this inequality into the expression for r_1, we obtain

$$r_1 < \alpha r_1, \tag{3.35}$$

which is a contradiction when $\alpha \leq 1$ and $r_1 > 0$. $\square$

3.3.1 Phase diagrams of equilibria without external fields

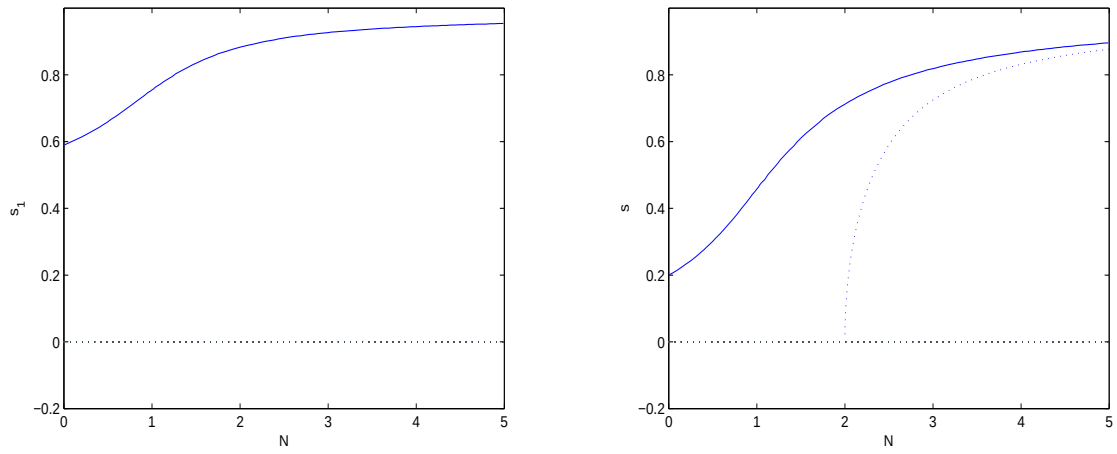

Figure 3.1: The bifurcation diagrams of s_1 and s are plotted against the dimensionless concentration N for $\alpha = 2.5$. Solid curves denote stable equilibria, while unstable equilibria are denoted by dashed curves. Three distinct branches of equilibria (s_1, s) are found. There exists a stable polar-nematic solution $(s_1 > 0, s > 0)$ for all N. The isotropic branch $(s_1 = s = 0)$ and the purely nematic branch $(s_1 = 0, s > 0)$ are unstable.

For $\alpha > 1$, new solution branches may exist and destabilize stable steady state so-

lutions which already exist for a purely nematic system. In this section, we will study steady state solutions obtained by solving (3.31), (3.32) numerically and construct bifurcation diagrams. We describe equilibria according to their two order parameters, s_1 and s, where $s_1 > 0$ is a polar phase and $s > 0$ is a nematic phase. States with $s_1 > 0$ and $s = 0$ do not exist; states with $s_1 = 0$, $s > 0$ are called non-polar, nematic; states with $s_1 > 0$, $s > 0$ are called polar nematic, and states with $s_1 = s = 0$ are non-polar and isotropic or simply isotropic. The stability is determined by examining the free energy density of the system:

$$A[f] = \int_{\|\mathbf{m}\|=1} [k_B T \ln f + \frac{V}{2}] f d\mathbf{m}. \tag{3.36}$$

From (3.28), we arrive at the free energy density at equilibrium:

$$\begin{aligned} A[f] &= \int_{\|\mathbf{m}\|=1} [-k_B T \ln Z - \frac{V}{2}] f d\mathbf{m} \\ &= -k_B T [\ln Z - \frac{\alpha s_1^2}{2} - \frac{N}{2}(s^2+1)], \qquad (3.37) \\ Z &= \int_{\|\mathbf{m}\|=1} e^{\alpha s_1 \cos\theta + N(s\cos 2\theta + 1)} d\mathbf{m}. \qquad (3.38) \end{aligned}$$

To guarantee stability of the solution, the eigenvalues of the Hessian matrix of the second variation of the free energy density must be positive. At the isotropic branch $(s_1 = 0, s = 0)$, the Hessian matrix is given by

$$\delta^2 A|_{s_1=0,s=0} = k_B T \begin{pmatrix} \alpha(1-\frac{1}{2}\alpha) & 0 \\ 0 & N(1-\frac{1}{2}N) \end{pmatrix}. \tag{3.39}$$

We thus conclude the isotropic equilibrium is unstable whenever $\alpha > 2$ or $N > 2$. It is well known that there is an isotropic-nematic transition at $N = 2$ and the isotropic branch loses stability beyond the transition point in a two-dimensional purely nematic system. In our numerical simulations, we observe that there exists a new stable solution branch for all N, if $\alpha > 2$. The existence of the new solution explains the loss of stability of the isotropic branch. Fig. 3.1 shows that there exists a new polar solution for all N at

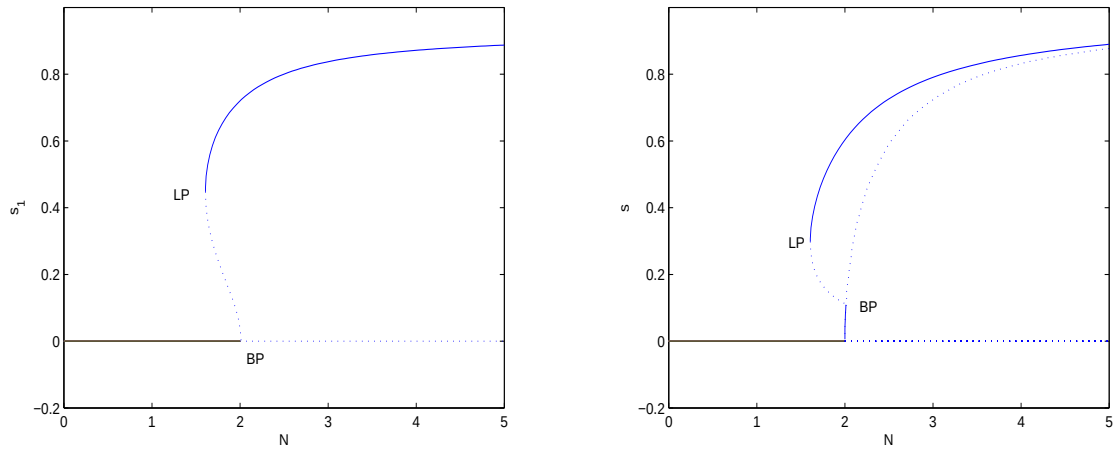

Figure 3.2: Bifurcation diagrams of s_1 and s are plotted against dimensionless concentration N for $\alpha = 1.8$. Solid (dashed) curves denote stable (unstable) equilibria. In addition to the isotropic-nematic transition at $N = 2$, there exist two bifurcation points at $N = 2.01$ (BP) where a new branch comes out of the purely nematic branch and $N = 1.61$ (LP) which is a turning point of the non-zero polar branch.

$\alpha = 2.5$. This suggests that if the strength of the dipole-dipole interaction is sufficiently high, the system is anisotropic regardless of the concentration N .

For the purely nematic branch ($s_1 = 0$, $s \neq 0$), the Hessian matrix is given by

$$\delta^2 A|_{s_1=0,s\neq 0} = k_B T \begin{pmatrix} \alpha(1 - \frac{1+s}{2}\alpha) & 0 \\ 0 & N(1 - N(< \cos^2 2\theta > -s^2)) \end{pmatrix}. \tag{3.40}$$

Let's say $g(s) = 1 - N(< \cos^2 2\theta > -s^2)$, then $g(0) = 0$ and $g'(s) > 0$ for all $s > 0$. Thus, $g(s)$ is positive for all $s > 0$. The critical value for α is

$$\alpha_1 = \frac{2}{1+s}, \tag{3.41}$$

beyond which the purely nematic branch is unstable. In other words, the purely nematic branch loses its stability beyond $s_c = -1 + \frac{2}{\alpha}$ for a given α. Since s is positive, the purely nematic solution is unstable for all $N > 2$, if $\alpha > 2$. Numerical solutions show that the critical point s_c is the point where the new branch comes out (BP).

The calculation of the Hessian matrix of a new polar solution branch reduces to a nu-

merical calculation.

We will give bifurcation diagrams of s and s_1 as a function of N for selected values of α using the continuation software AUTO 97 (Doedel *et al.*, 1998) and the above argument about stability.

Fig. 3.1 is the bifurcation diagram for $\alpha = 2.5$. The isotropic branch and the purely nematic branch are unstable. However, there exists a stable nonzero polar solution for all N.

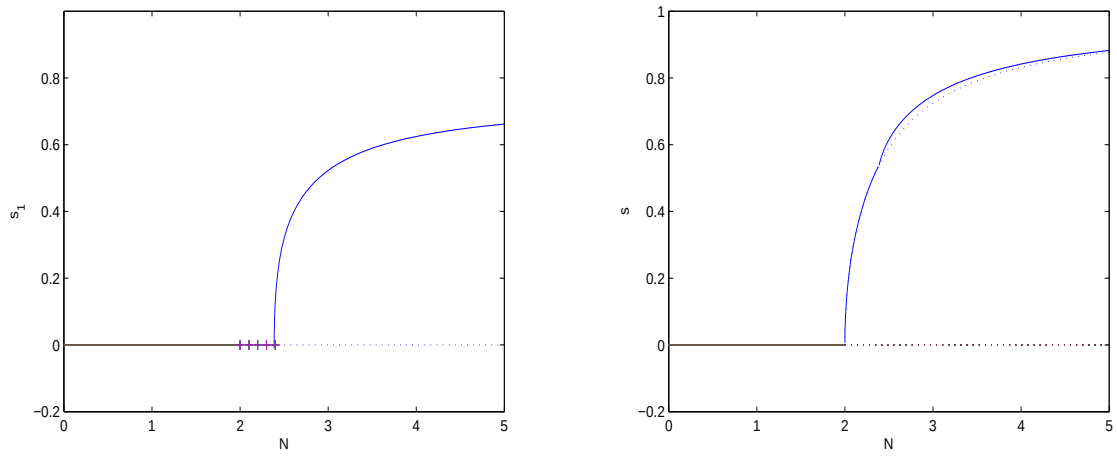

Figure 3.3: Bifurcation diagrams of s_1 and s are plotted against dimensionless concentration N for $\alpha = 1.3$. Solid (dashed) curves denote stable (unstable) equilibria. The non-zero polar solution branch starts at $N = 2.39$ (BP).

Fig. 3.2 is the bifurcation diagram for $\alpha = 1.8$. A non-zero polar solution branch bifurcates at $N_c = 2.01$, which is unstable. The nematic branch loses stability beyond N_c. The new polar branch becomes stable at a turning point $N_t = 1.61$. Thus, there exists bi-stability between $N = 1.61$ and $N = 2$

Fig. 3.3 depicts the bifurcation diagram for $\alpha = 1.3$. There exists an isotropic-nematic transition for the order parameter s at $N = 2$. A new stable branch comes out of the purely nematic branch at $N_c = 2.39$ due to the polarity. Beyond N_c, the purely nematic branch becomes unstable. The solution branch $s_1 = 0$ has multiplicity 2 between $N = 2$ and $N = 2.39$. One corresponds to a stable nematic solution branch of s and the other

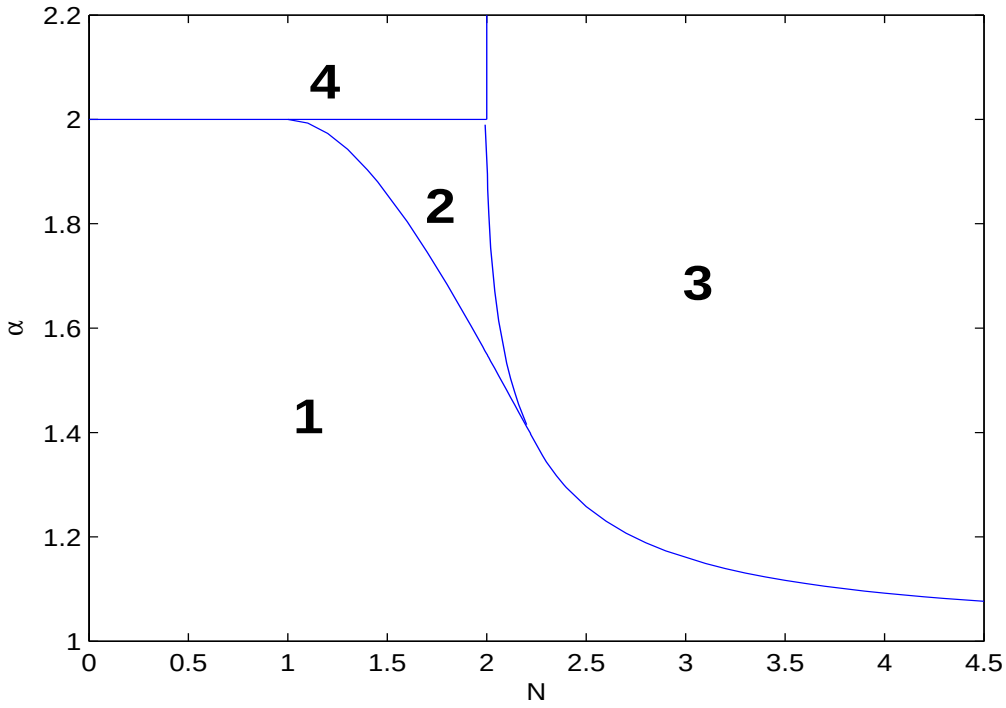

Figure 3.4: The parameter space is divided into 4 regions. The Region 1 is same with a purely nematic system. There exist a stable and unstable polar solution in the Region 2. There exists a polar solution in the Region 3 and 4.

branch corresponds to an unstable isotropic solution branch of s.

Now, we summarize the behavior of dipolar nano-rod dispersions under a dipolar interaction potential and an excluded-volume potential. Fig. 3.4 is the phase diagram of the dipolar nematic system in (N, α)-space. The parameter space is separated into 4 regions.

Region 1 In this region, a dipolar system has the same equilibria as a purely nematic system. There is no polar solution. The isotropic branch is stable if $N < 2$. If $N > 2$, there is a stable nematic branch and an unstable isotropic branch.

Region 2 In the Region 2, there exists bi-stability. There is a stable polar solution and an unstable polar solution. If $N > 2$, there exits a stable nematic branch and an unstable isotropic branch. If $N < 2$, there exist a stable isotropic branch.

Region 3 There exist a stable polar solution, an unstable nematic solution and an unstable isotropic solution.

Region 4 There exist a stable polar solution and an unstable isotropic solution.

3.4 Conclusion

In this chapter, we characterize all steady state solutions of magnetic nano-rod dispersions under general linear flows with a 2-parameter Boltzmann distribution. A pair of nonlinear integral equations must be solved instead of the infinite dimensional partial differential equation. We then construct bifurcation diagrams of equilibrium solutions of the Smoluchowski equation without external fields for a dipole-dipole interaction potential together with an excluded-volume potential. We determine the stability of solutions by examining the free energy density.

Appendix A

A.1 Closure approximations for 2D models

◦ Quadratic (Doi) Closure

$$(\bullet) :< \mathbf{mmmm} > \;=\; (\bullet) : \mathbf{MM}. \tag{A.1}$$

◦ Tsuji-Rey (TR) Closure

$$\begin{aligned}(\bullet) :< \mathbf{mmmm} > \;=\; & \tfrac{1}{4}[((\bullet) : \mathbf{Q})\mathbf{Q} + (\bullet) \cdot \mathbf{Q}^2 + \mathbf{Q} \cdot (\bullet) \cdot \mathbf{Q} + \mathbf{Q}^2 \cdot (\bullet) \\ & -(((\bullet) \cdot \mathbf{Q}) : \mathbf{Q})\mathbf{I}] + \tfrac{1}{2}((\bullet) : \mathbf{Q})\mathbf{I}.\end{aligned} \tag{A.2}$$

◦ Hinch-Leal 1 (HL1) Closure

$$\begin{aligned}(\bullet) :< \mathbf{mmmm} > \;=\; & \tfrac{1}{5}[6\mathbf{M} \cdot (\bullet) \cdot \mathbf{M} - (\mathbf{MM}) : (\bullet) \\ & -2((\mathbf{MM}) : (\bullet) - \mathbf{M} : (\bullet))\mathbf{I}].\end{aligned} \tag{A.3}$$

◦ Hinch-Leal 2 (HL2) Closure

$$\begin{aligned}(\bullet) :< \mathbf{mmmm} > \;=\; & \mathbf{M}(\mathbf{M} : (\bullet)) \\ & +2[\mathbf{M} \cdot (\bullet) \cdot \mathbf{M} - \mathbf{M}^2(\mathbf{M}^2 : (\bullet))/(\mathbf{I} : \mathbf{M}^2)] \\ & +\alpha(\mathbf{M})[\tfrac{52}{315}(\bullet) - \tfrac{8}{21}[(\bullet) \cdot \mathbf{M} + \mathbf{M} \cdot (\bullet) - (\mathbf{M} : (\bullet))\mathbf{I}]]\end{aligned} \tag{A.4}$$

where

$$\alpha(\mathbf{M}) = \exp[2(\mathbf{I} - 3\mathbf{M}^2 : \mathbf{I})/(\mathbf{I} - \mathbf{M}^2 : (\bullet))\mathbf{I}]]. \tag{A.5}$$

A.2 Model equations (s, θ) for each closure

◦ Quadratic Closure

$$\begin{aligned} \dot{s} &= 3s[N(1-s^2)-2] + aPe(1-s^2)\sin 2\theta, \\ \dot{\theta} &= -\tfrac{Pe}{2}(1-\tfrac{a}{s}\cos 2\theta), \\ s &= \sqrt{1-\tfrac{2}{N}}, \\ N_*(a) &= \tfrac{2}{1-a^2}. \end{aligned} \tag{A.6}$$

◦ Tsuji-Rey Closure

$$\begin{aligned} \dot{s} &= \tfrac{1}{8}(3s[N(8-5s^2)-16] + aPe(8-5s^2)\sin 2\theta), \\ \dot{\theta} &= -\tfrac{Pe}{2}(1-\tfrac{a(8-s^2)}{8s}\cos 2\theta), \\ s &= \sqrt{\tfrac{5}{8}(1-\tfrac{2}{N})}, \\ N_*(a) &= \tfrac{10+2a^2+5\sqrt{4+2a^2}}{10-4a^2}. \end{aligned} \tag{A.7}$$

◦ HL1 Closure

$$\begin{aligned} \dot{s} &= \tfrac{2}{5}(3s[N(1-s^2)-5] + aPe(1-s^2)\sin 2\theta), \\ \dot{\theta} &= -\tfrac{Pe}{2}(1-\tfrac{a(2+3s^2)}{5s}\cos 2\theta), \\ s &= \sqrt{1-\tfrac{5}{N}}, \\ N_*(a) &= \tfrac{5-6a^2+\sqrt{25-24a^2}}{2(1-a^2)}. \end{aligned} \tag{A.8}$$

◦ HL2 Closure

$$\begin{aligned} \dot{s} &= 2(3s[N\{\tfrac{68}{315}e^{6+\frac{16}{s^2-3}} + \tfrac{s^2}{1+s^2}(1-s^2)\} - 1] \\ &\quad + aPe[\tfrac{68}{315}e^{6+\frac{16}{s^2-3}} + \tfrac{s^2}{1+s^2}(1-s^2)]\sin 2\theta), \\ \dot{\theta} &= -\tfrac{Pe}{2}(1-\tfrac{a}{315}(136e^{6+\frac{16}{s^2-3}} + 315s^2)\cos 2\theta). \end{aligned} \tag{A.9}$$

A.3 Free energy density and its second variation

For the free energy density

$$A[f] = \int_{\|\mathbf{m}\|=1} [k_B T \ln f + \frac{V}{2}] f d\mathbf{m}, \tag{A.10}$$

its first and second derivatives are given by

$$\begin{aligned}
\frac{\partial A}{\partial s_1} &= \alpha k_B T(s_1 + < \cos\theta >) \\
\frac{\partial A}{\partial s} &= N k_B T(s + < \cos 2\theta >) \\
\frac{\partial^2 A}{\partial s_1^2} &= \alpha k_B T + \alpha^2 k_B T(s_1^2 - \tfrac{s+1}{2}) \\
\frac{\partial^2 A}{\partial s \partial s_1} &= -\alpha N k_B T(2 < \cos^3\theta > - s_1 - s s_1) \\
\frac{\partial^2 A}{\partial s^2} &= N k_B T[1 - N(< \cos^2 2\theta > - s^2)].
\end{aligned} \tag{A.11}$$

BIBLIOGRAPHY

Bhandar, A. S., and Wiest, J. M. (2003) "Mesoscale constitutive modeling of magnetic dispersions." *J. Colloid Interface Sci.*, **257**, 371-382.

Bird, R. B., Curtiss, C. F., Armstrong, R. C., and Hassager, O. (1987) *Dynamics of polymeric liquids, vol. 2, Kinetic theory.* Wiely, New York.

Chillingworth, D. R. J., Vicente Alonso, E., and Wheeler, A. A. (2001) "Geometry and dynamics of a nematic liquid crystal in a uniform shear flow." *J. Phys*, **34**, 1393-1404.

Cocchini, F., Aratari, C., and Marruucci, G. (1990) "Tumbling of rodlike polymers in the liquid-crystalline phase under shear flow." *Macromolecules*, **23**, 4446-4451.

Constantin, P., Kevrekidis I., and E. S. Titi, E. S. (2004) "Asymptotic states of a Smoluchowski equation." *Arch. Rat. Mech. Anal.*, **174**, 365-384.

Constantin, P., Kevrekidis, I., and Titi, E. S. (2004) "Remarks on a Smoluchowski equation." *Discrete and Continuous Dynamical Systems*, **11**, 101-112.

de Gennes, P. G., and Prost, J. (1993) *The physics of liquid crystals.* Oxford University Press, New York.

Doedel, E. J. *et al.* (1998) *AUTO 97: Continuation & bifurcation software for ordinary differential equations,* Concordia University.

Doi, M. (1981) "Molecular dynamics and rheological properties of concentrated solutions of rodlike polymers in isotropic and liquid crystalline phases." *J. Polymer Science*, **19**, 229-243.

Ericksen, J. L. (1983) *Orienting polymers: Proceedings, Minneapolis.* Springer-Verlag, Berlin Heidelberg.

Ermentrout, B. (2002) *Simulations, analyzing, and animating dynamical systems: A guide to XPPAUT for researchers and students.* SIAM, Philadelphia.

Faraoni, V., Grosso, M., Crescitelli, S., and Maffetone, P. L. (1999) "The rigid-rod model for nematic polymers: An analysis of the sher flow problem." *J. Rheol*, **43**, 829-843.

Fatkullin, I. and Slastikov, V. (2005) "Critical points of the Onsager functional on a sphere." *Nonlinearity*, **18**, 2565-2580.

Feng, J., Chaubal, C. V., and Leal, L. G. (1998) "Closure approximations for the Doi theory: Which to use in simulating complex flows of liquid crystalline polymers." *J. Rheol.*, **42**, 1095-1119.

Forest, M. G., and Wang, Q. (2003) "Monodomain response of finite-aspect-ratio macromolecules in shear and related linear flows." *Rheol Acta*, **42**, 20-46.

Forest, M. G., Wang, Q., and Zhou, H. (2000) "Exact banded patterns from a Doi-Marrucci-Greco model of nematic liquid crystal polymers." *Phys. Rev. E*, **61**, 6655-6662.

Forest, M. G., Zhou, R., and Wang, Q. (2003) "Full-tensor alignment criteria for sheared nematic polymers." *J. Rheol.*, **47**, 105-127.

Forest, M. G., Zhou, R. and Wang, Q. (2004) "Scaling behavior of kinetic orientational distributions for dilute nematic polymers in weak shear." *J. Non-Newtonian Fluid Mech.*, **116**, 183-204.

Forest, M. G., Sircar, S., Wang, Q., and Zhou, R. (to appear) "Monodomain dynamics for rigid rod & platelet suspensions in strongly coupled doplanar linear flow and magnetic fields II: kinetic theory." *Physics of Fluids.*

Golubitsky, M., and Schaeffer, D. G. (1985) *Singularities and groups in bifurcation theory*, Springer-Verlag, New York.

Grandner, S., Heidenreich, S., Ilg, P., Klapp, S., and Hess, S. (to appear) "Dynamic electric polarization of nematic liquid crystals subjected to a shear flow." *Physical Review Letters.*

Hess, S. (1976) "Fokker-Planck equation approach to flow alignment in liquid crystals." *Z. Naturforsch A*, **31**, 1034-1037.

Ji, G., Wang, Q., Zhang, P., and Zhou, H. (to appear) "A semi-analytic study of phase transition in rigid extended nematics and magnetic suspensions." *Physics of Fluids.*

Kawagucci, M. N. (1998) *Flow visualization and modeling of liquid crystalline polymers.* Ph.D. Dissertation, University of California, Berkeley.

Kupferman, R., Kawaguchi, M. N., and Denn, M. M. (2000) "Emergence of structure in a model of liquid crystalline polymers with elastic coupling." *J. Non-Newtonian Fluid Mech.*, **91**, 255-271.

Y. Kuznetsov, Y. (1995) *Elements of applied bifurcation theory.* Springer-Verlag, New York.

Kuzuu, N., and Doi, M. "Constitutive equation for nematic liquid crystals under weak velocity gradients derived from a molecular kinetic equation." *J. Phys. Soc. Japan*, **52**, 3486-3494.

Larson, R. G., and H. C. Öttinger, H. C. (1991) "Effect of molecular elasticity on out-of-plane orientations in shearing flow of liquid-crystalline polymers." *Macromolecules*, **24**, 6270-6282.

Maffetone, P. L., and Crescitelli, S. "The rigid rod model for nematic polymers: Testing closure approximations with bifurcation analysis." *J. Rheol.*, **38**, 1559-1570.

Maffetone, P. L., and S. Crescitelli, S. (1995) "Bifurcation anaylsis of a molecular model for nematic polymers in shear flow." *J. Non-Newtonian Fluid Mech.*, **59**, 73-91.

Maffetone, P. L., Grosso, M., Friedenberg, M. C., and Fuller, G. G. (1996) "Extensional flow of a two-dimensional polymer liquid crystal." *Macromolecules*, **34**, 8473-8478.

Marrucci, G., and Maffettone, P. L. (1989) "Description of the liquid crystalline phase of rodlike polymers at high shear rates." *Macromolecules*, **22**, 4076-4082.

Maffetone, P. L., and Marrucci, G. (1990) "Nematic phase of rodlike polymers. I. Prediction of transient behavior at high shear rates." *J. Rheol.*, **34**, 1217-1230.

Maffetone, P. L., and Marrucci, G. (1991) "A two-dimensional approach to the constitutive equation of nematic polymers." *J. Non-Newtonian Fluid Mech.*, **38**, 273-288.

Maruyama, T., Fuller, G. G., Grosso, M., and Maffetone, P. L. (1998) " The dynamics of two dimensional polymer nematics." *J. Non-Newtonian Fluid Mech.*, **76**, 233-247.

Onsager, L. (1949) " The effects of shape on the interaction of colloidal particles." *Annals of New York Academic of Sciences*, **51**, 627-659.

Platé, N. A. (1993) *Liquid-Crystal Polymers*. Plenum Press, New York.

See, H., Doi, M., and Larson, R. (1990) "The effect of steady flow fields on the isotropic-nematic phase transition of rigid rod-like polymers." *J. Chem. Phys.*, **92**, 792-800.

Strogatz, S. H. (2000) *Nonlinear dynamics and chaos*. Westview, Cambridge.

Vicente Alonso E., Wheeler A. A., and Sluckin, T. J. (2003) " Nonlinear dynamics of an nematic liquid crystal in the presence of a shear flow." *Pro. Roy. Soc. A.*, **459**, 195-220.

Wang, Q., Sircar, S., and Zhou, H. (2005). "Steady state solutions of the Smoluchowski equation for rigid nematic polymers under imposed fields." *Comm. Math. Sci.*, **3**, 605-620.

Yim, K. S., Fuller, G. G., Datko, A., and Eisenbach, C. D. (2001). " Isotropic-nematic phase transitions of lyotropic, two-dimensional liquid crystalline polymer solutions." *Macromolecules*, **34**, 6972-6977.

Zarnescu, A. (2006). "The stationary 2D Smoluchowski equation in strong homogeneous flow." *Nonlinearity*, **19**, 1619-1628.